Mohamed Khider University of Biskra
Faculty of exact sciences and natural and life sciences
Material sciences department

MASTER MEMORY

Domain of Matter Sciences
Section of Physics
Speciality of Materials Physics
Réf. :

Prsentedd by:
Nezzal Hala & Redjouh Nour El Houda

The: 26/6/2022

Elaboration of pure and Bi-doped ZnO nano-powders with the sol-gel method

---

Jury:

Mrs.	Guergueb saida	MAA	University Med Khidar of Biskra	Presidant
Ms.	Arab Louiza	MCA	University Med Khidar of Biskra	Reporter
Mrs.	Almi Kenza	MCB	University Med Khidar of Biskra	Examiner

Academic Year: 2021/2022

ACKNOWLEDGEMENTS

Firstly, we thank Almighty Allah, who gave us the courage and strength to carry out our work. Our highest praise goes to him for the health and patience he has bestowed on us throughout our years of study.

Then, we would like to express our deepest love, respect, and admiration to our families for their unconditional support, understanding, and dedication throughout these years.

We are also thankful to our supervisor ***Dr. Louiza Arab*** *for the continual follow-up throughout the realization of this memory, and who has not stopped giving us her advice and comments.*

We warmly thank the jury members: ***Dr. Guergueb saida*** *and* ***Dr. Almi Kenza*** *For agreeing to review our work.*

We take immense pleasure in expressing our deep gratitude to Prof. ***Saad Rahmane*** *and Prof.* ***Abdlouahed Chala*** *for their unstinted guidance and constant encouragement and kind help extended to our work.*

We owe our heartful thanks to ***Ms. Aya Latif****, without her continuous support this study would not have been completed.*

Lastly, we offer our regards to many people who, from near or far, have contributed to the achievement of this work.

Thank you...

Hala & Houda

DEDICATION

From the bottom of my heart, I dedicate this work to all those who are dear to me,

To my parents, my sister, my brothers and, my entire family

To everyone who contributed in this humble work

With a lot or a little

To my friends and all the people who supported me

May Allah reward you with all goodness

Nour Houda Redjouh

DEDICATION

From the bottom of my heart, I dedicate this work to all those who are dear to me,

To my parents, my sisters and, my entire family

To everyone who contributed in this humble work

With a lot or a little

To my friends and all the people who supported me

May Allah reward you with all goodness

Hala Nezzal

LIST OF CONTENT

Acknowledgements:.....II

Dedication:……III

List of figures:……XI

List of tables:……XIII

GENERAL INTRODUCTION:……...1

Chapter one: Bibliographic studies

I.1.Introduction:……..3

I.2.History of Zinc oxide (ZnO) research:……..3

I.3.Properties of zinc oxide:……4

I.3.1.Physical Properties:……..4

I.3.1.1.Crystal structure:……5

I.3.1.2.Electronic band structure:……7

I.3.1.3.Electrical Properties:……8

I.3.1.4.Optical Properties:……...9

I.3.1.5.Mechanical Properties:……..10

I.3.1.6.Piezoelectric effect:……...10

I.3.2.Chemical Properties:……11

I.4.Applications of zinc oxide:……..12

I.4.1.Rubber manufacture:……12

I.4.2.Medical uses:……12

I.4.3.Food additives:……..13

I.4.4.Anti-corrosive coatings:……13

I.4.5.Electronic applications:……13

I.4.6.Varistors:……..14

I.5. Properties of zinc oxide Nanostructures:……..14

I.5.1.Morphology Controlled:……..14

I.5.2.Physico-chemical Properties:……...15

I.5.2.1.Nanobelts:……15

I.5.2.2.Nanowires:……16

I.5.2.3.Nanorods:……..16

I.6.Advantages of zinc oxide:……..16

REFERENCES:……17

Chapter two: Methods and materials

II.1.Introduction:……...19

II.2.Synthesis of Inorganic Nanomaterials:……...19

II.3.Sol-Gel process:……20

II.3.1.Introduction:……20

II.3.2.An overview of sol-gel process steps:……20

II.3.2.1.Hydrolysis and condensation:……20

- Hydrolysis reaction:……...20
- Condensation reaction:……..20

II.3.2.2.Gelation:……21

II.3.2.3.Ageing:……..21

II.3.2.4.Drying:……...21

II.3.2.5.Densification:……22

II.3.3.Major control parameters of sol-gel process:……...22

II.3.3.1.Chemical compositions of the precursors:……23

II.3.3.2.Hydrolysis ratio:……23

II.3.3.3.Catalysts:……...24

II.3.3.4.pH value:……...24

II.3.3.5.Reaction temperature:……24

II.3.4.Advantages and shortages of sol-gel processing:…….24

II.3.5.Applications of Sol Gel method:……26

II.4.Synthesis of pure and Bi doped zinc oxide powder:…….27

II.4.1.Experimental conditions:…….27

II.4.2.Experimental details:……28

II.4.2.1.Pure ZnO nano-powders:…….28

II.4.2.2.Bi-doped ZnO nano-powders:…….28

II.4.3.Calcination treatment:……..30

II.5. ZnO powder characterization techniques:…….32

II.5.1.Structural characterization:……...32

II.5.1.1.X-ray diffraction (XRD):…….32

II.5.1.2.Determination of the grains size:…….33

II.5.1.3.Determination of the interreticular distances and the cell parameters:……34

II.5.1.4. Determination of the lattice strain and the dislocation density:……..34

II.5.1.5. Determination of texturing coefficients:…….35

II.5.2.Optical characterization:……...35

II.5.2.1.The Optical Gap:……..36

II.5.2.2.The Absorption Coefficient:……37

II.5.2.3.Urbach energy:…….38

II.5.2.4. Sample preparation:……39

II.5.3.Chemical characterization:……...39

II.5.3.1.Fourier Transform Infrared Spectroscopy (FTIR):……..39

II.5.3.2.Sample preparation:…….40

REFERENCES:……..41

Chapter three: Results and discussions

III.1. Introduction:……43

III.2. Results and discussions:……43

III.2.1. Structural study:……43

III.2.1.1.Crystallite size, lattice strain and dislocation density variation:……47

III.2.1.2.Lattice parameters:……50

III.2.1.3.The texture coefficient:……52

III.2.2.Optical study:……53

III.2.2.1.Band gap energy:……54

III.2.2.2.Urbach energy:……55

III.2.3.Chemical study:……57

REFERENCES:……59

GENERAL CONCLUSION:……61

Abstract

LIST OF FIGURES

Figure I.1	Increase of the number of publications about zinc oxide accordingto the literature database SCOPUS……..	04
Figure I.2	Models showing (i) the rocksalt, (ii) zinc blende, and (iii) wurtzite crystal structures of ZnO…….	05
Figure I.3	Representation of (I) ZnO wurtzite crystal structure, (II) atomic Structureof wurtzite-closed circle, open circle, and thick solid line represent cation, anion, and projection of two bonds, respectively……...	06
Figure I.4	Band structure and symmetries of hexagonal ZnO……..	07
Figure I.5	Ball and stick model of the relaxed atomic positions of interstitial hydrogen: (a) at the bond-center site parallel to the c axis; (b) at the antibonding sitePerpendicular to the c axis; (c) at the substitutional oxygen site…….	08
Figure I.6	Band diagram illustrating different processes that make up the photoluminescence spectra, excitation relaxation, and recombination in k-space……..	09
Figure I.7	Various ZnO nanostructures. Note: Scale bar is not shown……..	15
Figure II.1	Top-down and bottom-up approach for the synthesis of nanoparticles….	19
Figure II.2	Steps of the sol gel process of materials and examples of the microstructure of final products. Bold-lined rectangles show possible final products of the sol gelmethod……..	22
Figure II.3	Applications of sol gel method…….	26
Figure II.4	Pure and Bi-doped ZnO powders……..	29
Figure II.5	Nabertherm oven……...	30
Figure II.6	Flowchart of the synthesis of pure and Bi doped ZnO nanopowders using sol gel method……..	31
Figure II.7	The Principle of Bragg's Law……	32
Figure II.8	The Rigaku MiniFlex 600 diffractometer……..	33
Figure II.9	Schematic of the system for XRD measurements……	34
Figure II.10	EVOLUTION 220 spectrophotometer image……	36
Figure II.11	Determination of Eg……..	37
Figure II.12	Determination of the disorder by extrapolation starting from the variation ofLn (α) has in function of hν…….	38
Figure II.13	Schematic diagram of the operational principle of the Michelson interferometer……	39
Figure II.14	Transparent granules of pure and doped zinc oxide……..	40
Figure III.1	XRD pattern of undoped ZnO powders……	43
Figure III.2	XRD pattern of Bi-doped ZnO with a doping concentration of 3%.....	44
Figure III.3	XRD patterns of Bi-doped ZnO with a doping concentration of 6%.....	44
Figure III.4	XRD patterns of Bi-doped ZnO with a doping concentration of 8%.....	45
Figure III.5	Peak positions of the standard ZnO……...	46
Figure III.6	Variation of the intensity of the (002) peak……...	47
Figure III.7	Crystallite size and the strain as functions of Bi-doping……...	49

Figure III.8 The dislocation density as functions of Bi-doping…… 50
Figure III.9 Variation of lattice parameters with Bi-doping……. 52
Figure III.10 The transmittance spectra of undoped and Bi doped ZnO…… 53
Figure III.11 Plots of $(\alpha h\nu)^2$ versus E of pure and Bi doped ZnO…….. 54
Figure III.12 Variation of the band gap with the Bi doping…… 55
Figure III.13 Plots of ln(α) against E of pure and Bi doped ZnO……... 56
Figure III.14 Urbach energy as function of the Bi doping…….. 57
Figure III.15 FTIR spectra of undoped ZnO and Bi-doped ZnO…… 58

LIST OF TABLES

Table I.1	Physical properties of the zinc oxide in the wurtzite form…….	11
Table II.1	The physical and chemical properties of different chemicals used in thiswork……...	27
Table II.2	Experimental conditions for the production of pure and Bi-dopedZnO nanopowders……	30
Table III.1	A summary table of the structural parameters of pure and Bi-doped ZnO.	48
Table III.2	Lattice parameters of pure and Bi-doped ZnO powders…….	51
Table III.3	Texture coefficient values for pure and Bi-dopedZnO……...	52
Table III.4	Optical band gap values of undoped and Bi doped ZnO…….	55
Table III.5	Urbach energy values of undoped and Bi doped ZnO……	57

GENERAL INTRODUCTION

Significant technological developments over the past decade have changed the way we live, work and interact with each other. Every year, experts make predictions about the emerging technologies, for example in the future, advanced optoelectronic devices are expected to have small sizes, high performance, and high operation speeds. Nanostructured semiconductor materials are appropriate to realize these goals because they have some unique physical, chemical and optical properties as well as an interesting size. Therefore, they can be widely applied in optoelectronics, medicine, photocatalyst, electronics, and photonics.

Zinc oxide (ZnO), a wide-band gap semiconductor with a direct energy gap about 3.37 eV, has emerged as one of the most promising metal oxide nanomaterials for practical applications in the above mentioned fields, due to its optical and electrical properties, high chemical and mechanical stability, in addition to its large availability and low cost [1].

The modification of ZnO properties by doping has become an important research topic in order to improve the intrinsic characteristics of the base material. In such context, we report a study on ZnO and Bi-doped ZnO nanopowders synthesized via the sol-gel process. This method provides an efficient and cost-effective platform and produces samples with high purity, homogeneity, and a structure of easy control.

The purpose of This work is to check the effect of Bi on ZnO in view of a possible use of the doped nanostructures for various applications.

To provide a common footing for the chapters that follow, the first chapter consists of a brief survey on the main proprieties, advantages, and applications of zinc oxide.

The second chapter introduces the sol-gel method's definition, steps, advantages and applications. Then a detailed procedure for the preparation of undoped ZnO powders as well as the Bi-doped ones is presented. Finally the various characterization techniques employed in this study are given.

The third and final chapter presents and discusses the characterization results of Zinc oxide powders doped with bismuth. An interpretation of the impact of the Bi doping concentration on the structural and optical properties of ZnO is included.

This work ends with a general conclusion that highlights the major outcomes and some future outlooks about the obtained results.

References:

[1] T. Prakash, G. Neri, A. Bonavita, E. Ranjith Kumar, K. Gnanamoorthi, Structural, morphological and optical properties of Bi-doped ZnO nanoparticles synthesized by a microwave irradiation method, p 4913–4921, 2015.

Chapter I : bibliographic studies

I.1. Introduction:

In recent years, the (II-VI) semiconductors' growth and it characterization, such as ZnO, has been highlighted mainly as an active study subject. Both the scientific significance and the possibility for a variety of practical applications have fueled the research efforts.

The first chapter will tackle the main proprieties, applications and advantages of zinc oxide.

I.2. History of Zinc oxide (ZnO) research:

ZnO is not "a new semiconductor", it has a considerable history of studies dealing with its growth techniques and characterization of its material properties, which has been investigated already since 1912. With the start of semiconductors era after the invention of the transistor, lattice parameters of ZnO are known from 1935, whereas detailed values of optical parameters were accessible in the middle of the 50s. Systematic research of ZnO as a compound semiconductor was carried out in 1960.

After intensive study phases in the 1950s and 1970s, ZnO as a semiconducting material is currently experiencing a revival. Despite the fact that good quality thin films were manufactured in 1970 (by chemical vapor deposition), ZnO has just recently gained popularity. Since about 1990, an increase in the number of publications on ZnO occurred (see Figure I.1) and more recent reviews on ZnO have been published.

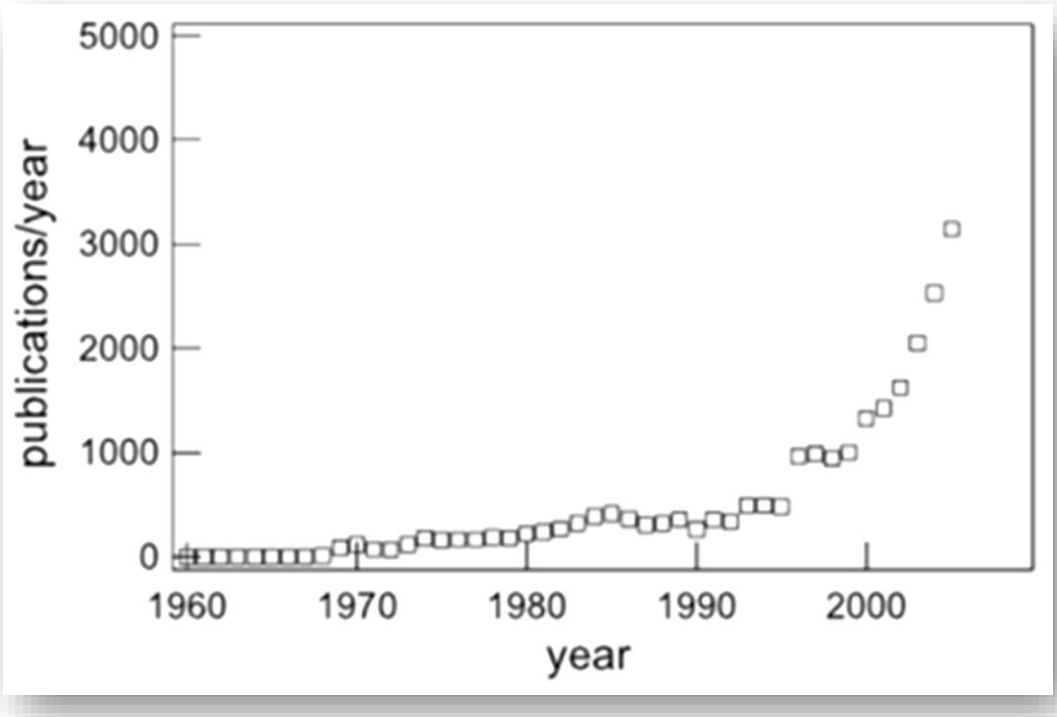

Figure I.1: Increase of the number of publications about zinc oxide according to the literature database SCOPUS [1].

I.3. Properties of zinc oxide:

Zinc oxide (ZnO) is a direct band gap semiconductor with great potential for a variety of applications, such as: optical waveguides, phosphors, transparent conductive oxides, chemical gas sensors, spin functional devices, UV-light emitters, and piezoelectric transducers. Its wide band-gap (3.37 eV at room temperature) makes ZnO a promising material for optoelectronic and photonic applications in the UV, or blue spectral range [2].

These various applications are linked to zinc oxide proprieties, as:

I.3.1. Physical Properties:

The physical properties of ZnO are as follows [3]:

- Molecular Weight: 81.37 g/mole.
- Color: Pure microcrystalline zinc oxide is white. Single crystal zinc oxide is colorless. Zinc oxide turns lemon yellow on heating and reverts to white on cooling.
- Relative Density: 5.607

- Melting Point: Zinc oxide sublimes at atmospheric pressure at temperatures over 1200°C. Under high pressure, a melting point of 1975 °C has been estimated.
- Refractive Index : w = 2.004, e = 2.020
- Heat of Sublimation between 1350 °C and 1500 °C: 193 Kcal/mole (vapor associated).
- Heat Capacity: Cp = 9.62 cal/deg/mole at 25 °C.
- Coefficient of Thermal Expansion $=4*10^{-6}$ $°C^{-1}$.

I.3.1.1. Crystal structure:

ZnO is a group of (II–VI) binary compound semiconductor that usually crystallizes in one of these three forms: hexagonal wurtzite, cubic zincblende, or cubic rocksalt (or Rochelle salt) as schematically indicated in (Figure I.2). The zinc blended ZnO symmetry can be stabilized only by growth on cubic substrates, whereas the rocksalt or Rochelle salt may be observed at relatively high pressures. The crystal structure of ZnO at the nanoscale is wurtzite, hence it is the most common form at ambient conditions. Due to the fact that it is a non-centrosymmetric (I,e. it has no inversion symmetry), the ZnO crystals have piezoelectricity and pyroelectricity properties.

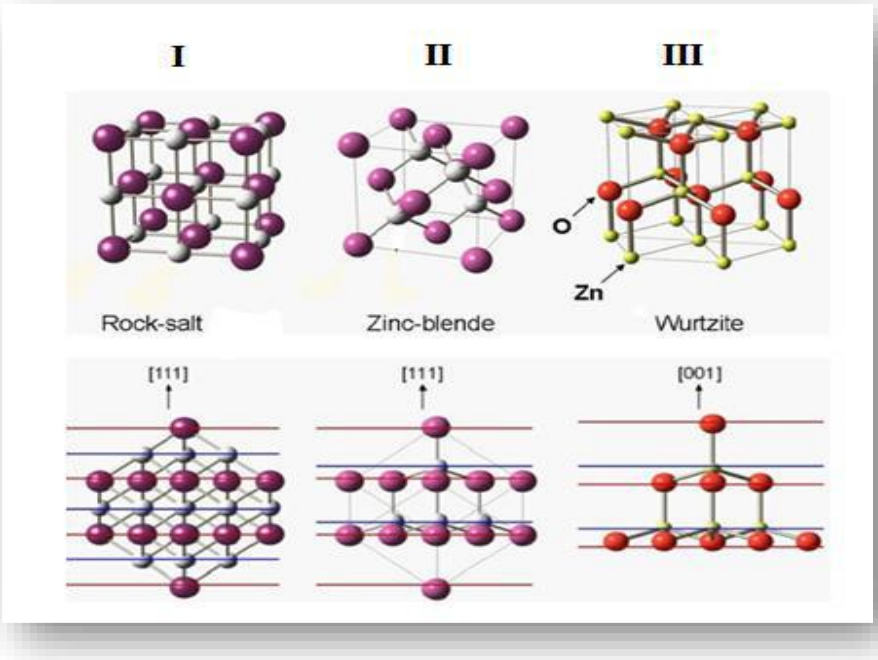

Figure I.2: Models showing (i) the rocksalt, (ii) zinc blende, and (iii) wurtzite crystal structures of ZnO [4].

The ZnO wurtzite structure has a hexagonal unit cell with two lattice parameters a=0.32 nm and c = 0.520 nm in the ratio of c/a = 1.633. The ZnO wurtzite structure belongs to the space group C_{6V}^4 in the Schoenflies notation and P6₃mc in the Hermann-Mauguin notation. (Figure I.3) clearly shows the structure composed of two interpenetrating hexagonal close-packed (hcp) sublattices, (where O^{-2} and Zn^{+2} ions are tetrahedrally-coordinated with each other). Each sublattice consists of one type of atom (Zn or O) displaced concerning each other along the threefold c-axis by the amount of u = 3/8 = 0.375 (in an ideal wurtzite structure) in fractional coordinates. Moreover, each sublattice consists of four atoms per unit cell, and every group II atom is surrounded by four atoms of the group VI atom or vice versa. The oppositely charged ions produce positively charged Zn-(0001) and negatively charged O-(000$\bar{1}$) surfaces resulting in a normal dipole moment and spontaneous polarization along the c-axis as well as a divergence in surface energy. Many ZnO properties such as growth, etching, defect generation and plasticity, spontaneous polarization, and piezoelectricity depend on its polarity [5].

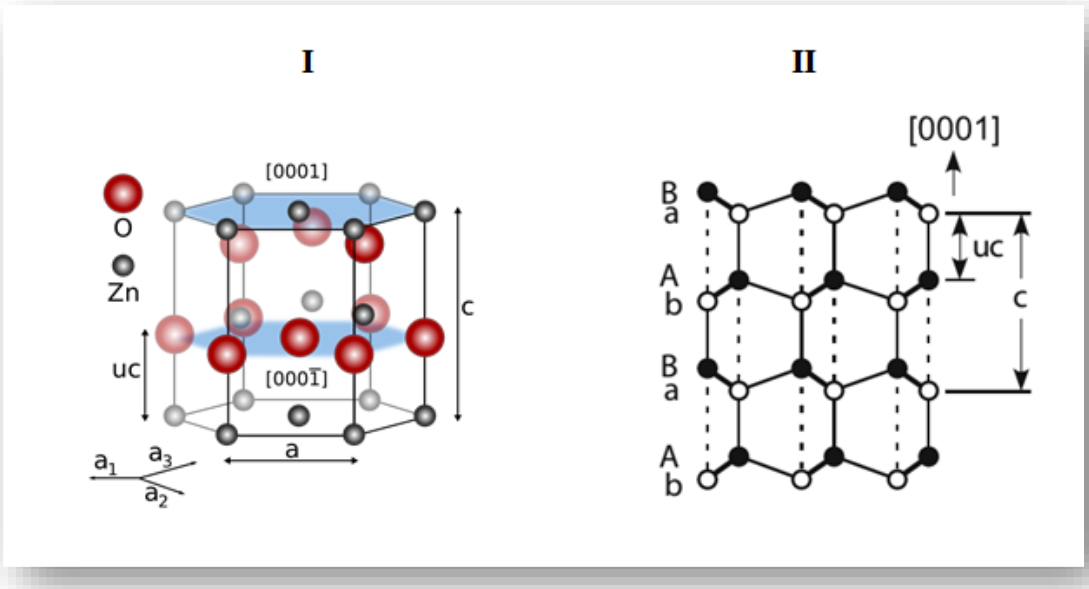

Figure I.3: Representation of (I) ZnO wurtzite crystal structure, (II) atomic structure of wurtzite-closed circle, open circle, and thick solid line represent cation, anion, and projection of two bonds, respectively [6].

The pairs of cation and anion atoms in the wurtzite structure (connected by dashed lines along with the [0001] direction in (Figure I.3 (II)) are attracted to each other by electrostatic force. It is considered that these electrostatic interactions allow the wurtzite-ZnO to be more stable than the zincblende-ZnO. Additionally, the (0001) polar plane which is associated with the direction <0001> commonly used for growth, so many other ZnO secondary planes and directions exist in the crystal structures [7].

I.3.1.2. Electronic band structure:

So far, the coherence between theoretical calculation and experiments for energy band structure has already been achieved for a great number of semiconductors, including ZnO of course. Since excellent and detailed optical data has been available in various cases.

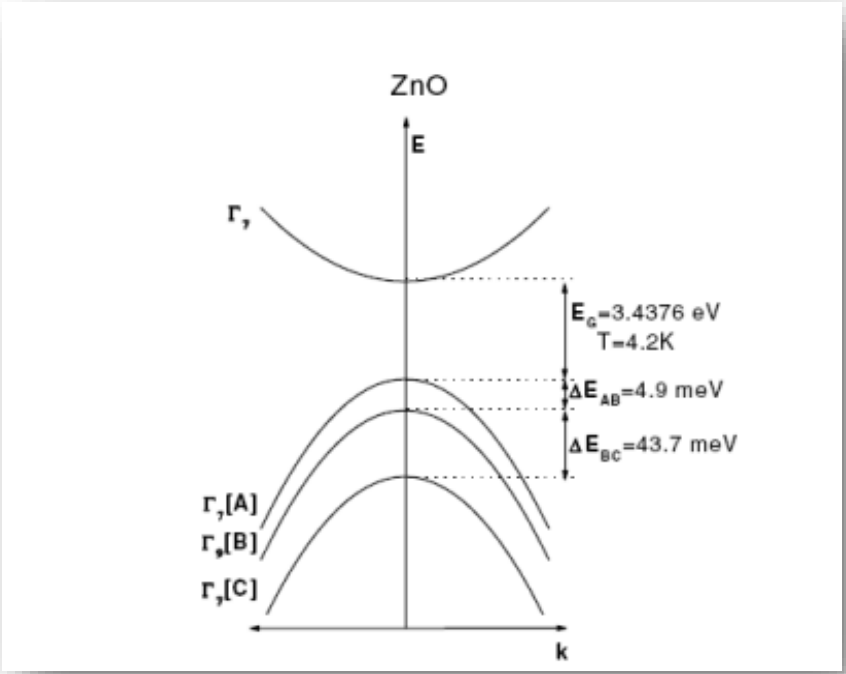

Figure I.4: Band structure and symmetries of hexagonal ZnO [8].

It is worth noting that the ZnO valence band is split experimentally by crystal field and spin-orbit interaction into three states named A, B, and C under the wurtzite symmetry. This splitting is schematically illustrated in (Figure I.4). The A and C sub-bands are known to possess Γ_7 symmetry, whilst the middle band, B, has Γ_9 symmetry.

I.3.1.3. Electrical Properties:

ZnO mostly exists as an n-type semiconductor, whose frequently observed unintentional n-type conductivity was supposedly believed to be due to the existence of native point defects that is attributed to the oxygen vacancies and Zn interstitial ions, which act as donors in the ZnO lattice. Recent researches indicate that oxygen vacancies are deep rather than shallow donors and it cannot cause the observed n-type conductivity. The course would be related to the unintentional incorporation of donor impurities that act as shallow donors, with hydrogen being a likely candidate. Furthermore, It has been confirmed that both the interstitial and substitutional hydrogen act as shallow donors in ZnO. The interstitial hydrogen forms a strong bond with O in ZnO, and it performs as a shallow donor contrary to its amphoteric behavior in controversial semiconductors and diffuses easily. Interstitial hydrogen prefers sites where it can strongly bind to an oxygen atom, forming an O-H bond length of (0.99 - 1.01) Å, as shown in (Figures I.5 (a) and (b)). On the other hand, the substitutional hydrogen on an oxygen site (observed in Figure I.5 (c)) diffuses easily and can alternatively be regarded as a complex consisting of hydrogen and an oxygen vacancy [9, 10].

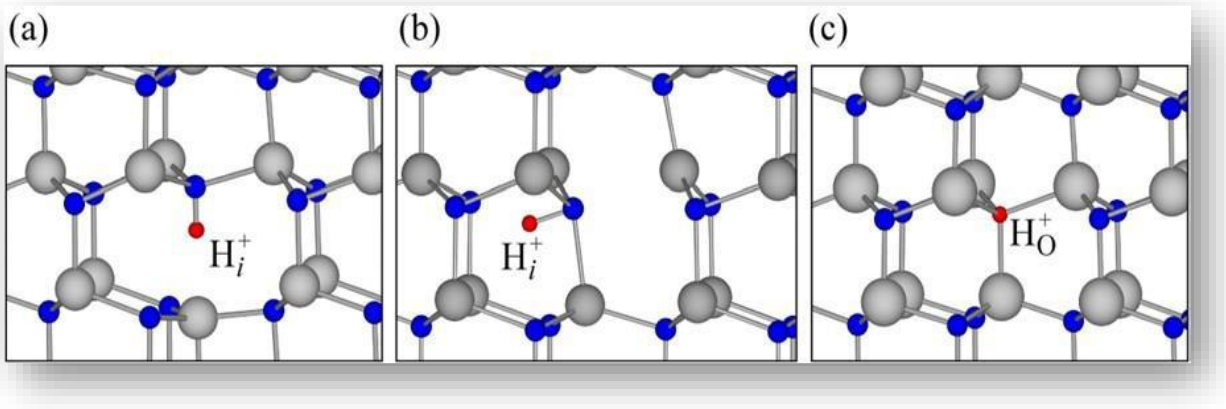

Figure I.5: Ball and stick model of the relaxed atomic positions of interstitial hydrogen: (a) at the bond-center site parallel to the c axis; (b) at the antibonding site perpendicular to the c axis; (c) at the substitutional oxygen site [11].

I.3.1.4. Optical Properties:

A variety of experimental techniques have been used to investigate optical transitions in ZnO, including optical absorption, reflection, photoluminescence, transmission, cathodoluminescence, and so on. At room temperature, the photoluminescence (PL) spectrum of ZnO typically consists of a UV emission band and a broad emission band. Luminescence is light emission by any process other than heating. Luminescence in semiconductors is the direct result of electron transitions from higher to lower energy levels. (Figure I.6) highlights a simplified band structure of a semiconductor near the center of the first Brillouin zone where a material with band gap energy Eg is irradiated by light or heat with energy $h\nu > E_g$, resulting in the excitation of an electron. The electron and hole thermalize to the lowest energy state of their respective bands via photon emission. Before recombining across the fundamental band gap or defect levels within the band gap, they emit photons of the corresponding energies.

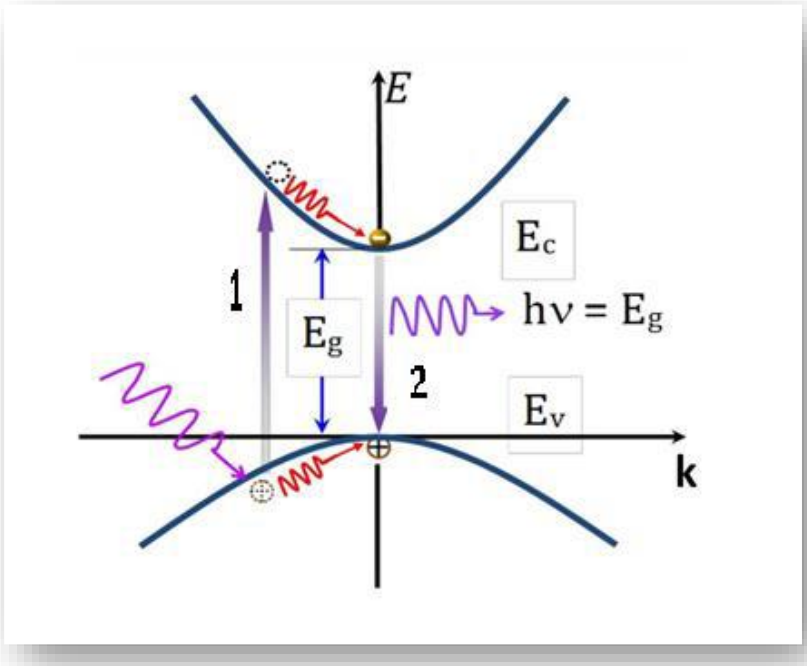

Figure I.6: Band diagram illustrating different processes that make up the photoluminescence spectra, excitation relaxation, and recombination in k-space [12].

The optical properties of a semiconductor are associated with both intrinsic and extrinsic effects. Intrinsic effects take place between the electrons in the conduction band and the holes in the valence band, including excitonic effects caused by the Coulomb interaction. Extrinsic

effects are related to dopants/ impurities or point defects and complexes, which usually create electronic states in the band-gap; therefore, they impact both optical absorption and emission processes.

I.3.1.5. Mechanical Properties:

ZnO is extremely such a soft material with an approximate hardness of just 4.5 on the Mohs scale. Its elastic constants are relatively smaller than those of other III-V semiconductors, for example. GaN. The high heat capacity and high heat conductivity, low values of thermal expansion, and high melting points are some of ZnO's characteristics. This latter has been proposed to be a more promising UV emitting phosphor than GaN because of its larger exciton binding energy (60 meV). Among the semiconductors bonded tetrahedrally, it was found that ZnO has the highest piezoelectric tensor. Consequently, it becomes a significant material for many piezoelectric applications, which require a high degree of electromechanical coupling among them [3].

I.3.1.6. Piezoelectric effect:

The piezoelectricity of ZnO has been widely researched for various applications in force sensing, acoustic wave resonator, acoustic-optic modulator…etc. The origin of piezoelectricity lies due to its crystal structure, in which the oxygen atoms and zinc atoms are tetrahedrally bonded. In such a noncentrosymmetric structure, the center of both positive and negative charge can be displaced due to externalpressure-induced lattice distortion. This displacement results in local dipole moments, thus a macroscopic dipole moment appears over the entire crystal. In fact, among the tetrahedrally bonded semiconductors, ZnO has the highest tensor which provides a large electro-mechanical coupling [3].

Table I.1: Physical properties of the zinc oxide in the wurtzite form [13].

Property	Value
Lattice constants (T=300K) **a_0 (nm)** **c_0 (nm)** **a_0/c_0**	 0.32495 0.52069 1,602 (1,633 in an ideal wurtzite structure)
Density (g/cm^3)	5.606
stable structure (T=300K)	Wurtzite
Melting point (K)	2248
Relative dielectric constant	8.66
Refractive index	2.008-2.029
Gap Energy (eV), direct	3.4
Intrinsic carrier concentration (cm^{-3})	< 106
Exciton binding Energy (meV)	60
Electron effective mass (Kg)	0.24 m_0
Electron Hall mobility at (T=300K) for low n-type Conductivity (cm^2/V.s)	200
Hole effective mass (Kg)	0.59 m_0
Hole Hall mobility at (T=300K) for low p-type conductivity (cm^2/V.s)	5-50

I.3.2. Chemical Properties:

ZnO has the following chemical properties [3]:

- ZnO occurs as the mineral zincate or as white powder known as zinc white. It is usually orange or red due to manganese impurity.
- Crystalline zinc oxide is thermochromic, that changes from white to yellow color when heated and reverting to white on cooling. This color change is caused by a very small loss small loss of oxygen at high temperatures.
- Zinc oxide is amphoteric, that reacts with both acids and alkalis. With acid, it reacts to form familiar compounds, such as zinc sulfate. Alkaliforms zincates.

$$ZnO + 2HCl \rightarrow ZnCl_2 + H_2O$$

$$ZnO+2NaOH+H_2O \rightarrow Na_2(Zn(OH)_4)$$

- ZnO decomposes to form zinc vapor and oxygen at about 1975 ˚C, indicating its considerable stability. Heating with carbon converts ZnO into Zn, which is more volatile.

$$ZnO+C \rightarrow Zn+CO$$

- The following reaction is extremely important in zinc pyrometallurgy.

$$ZnO+CO \rightarrow Zn+CO_2$$

- Commercial zinc oxide shows a measurable but low level of water solubility, 0.005 g/litre.
- Zinc oxide exposed to air absorbs both water vapor and carbon dioxide. This results in the formation of basic zinc carbonate.

I.4. Applications of zinc oxide:

ZnO has a diverse range of applications. Due to its reactivity, ZnO is an excellent precursor for obtaining other Zn compounds. ZnO has proven to be a boon to materials science because of its various advantages, for instance: UV absorption, antimicrobial capabilities, and steady thermal and optical properties. ZnO has made a substantial contribution to ceramics, lubricants, ointments, adhesives, and the rubber sector [14].

I.4.1. Rubber manufacture:

The rubber industry is responsible for consuming about 50% of the ZnO that is produced globally. ZnO along with stearic acid is a must for activating the process of vulcanization in rubber manufacture. Rubber curing becomes faster and more controlled when a combination of these two substances is utilized. It is also a crucial additive in car tires. It assists in improving their thermal conductivity which helps the tires to dissipate heat quickly when they are in motion thereby increasing their life span.

I.4.2. Medical uses:

A mixture of ZnO with 0.5% Fe_2O_3 is known as Calamine and is used in manufacturing Calamine lotions. Fine particles of ZnO have anti-microbial and deodorizing qualities, hence they are used for packaging purposes. These properties along with their ability to neutralize acids make it ideal for use in creams, like: antiseptic, healing, and so on. Additionally, they are

also an essential component of toothpaste and dental prosthetics. Due to its ability to absorb ultraviolet light, ZnO is used in sunscreens and sun blocks to prevent sunburns. The ZnO is also used in the production of cigarette filters as it is helpful in removing harmful substances like H_2S and HCN without affecting the flavor.

I.4.3. Food additives:

ZnO is usually added to food products as a source of Zn which is considered to be a necessary nutrient, as it helps in the performance of various physiological activities like growth and proper functioning of the sexual organs. Besides, it is also adjoined to fodder as a Zn supplement for livestock. Zinc oxide is used to manufacture zinc gluconate that is nowadays found in cold prevention lozenges.

I.4.4. Anti-corrosive coatings:

Zinc oxide is an excellent inhibitor of fungi, mildew, and mold. Paints, are usually used as anti-corrosive coatings for various metals like galvanized Zn which is especially hard to protect, as it allows to produce organic coatings brittle and unsuitable for adhesion. ZnO paints, on the other hand, maintain their flexibility and adhesive properties for years on end. The UV blocking abilities of ZnO also play a significant role in enhancing the paint's. Unlike some lead pigments that are available commercially, ZnO is impervious to the effect of sulfur compounds that are present in the atmosphere.

I.4.5. Electronic applications:

The wide band-gap of ZnO enables it to be used to make LEDs and laser diodes. Transparent thin-film transistors (TTFT) can also be produced with ZnO. Nanorod sensors made of ZnO are devices that detect fluctuations in electric current passing through the wires as a result of the adsorption of gas molecules. Moreover, the nanorods can be made partial towards H_2 gas by sputtering Pd clusters on the surface, which helps in dissociating the H_2 molecules thereby boosting the sensitivity of the nanorods. H_2 concentrations up to 10 ppm can be detected at room temperature without any response to O_2. Properties like biocompatibility have enabled ZnO to be used as a biomimetic material in order to modify and immobilize biomolecules. As Field-effect transistors (FETs), they can function without even a pn junction thus by passing doping problems. This is why some FETs use nanorods made of ZnO as conducting channels. ZnO is also used in making Zn-C dry cells, Ni-Cd oxide batteries, Zn-Ag oxide batteries, and also some secondary batteries. Another major area of ZnO

application is fuel cell where it is utilized to make various parts like the electrodes and sometimes also as the fuel. It can also act as a photo catalyst in places like the solar cell.

I.4.6. Varistors:

ZnO varistors have been widely used as surge protectors in electrical transmissions and circuits against lightning or transient overvoltage. These applications are due to their nonlinear electrical characteristics originating from the grain boundaries. The ZnO-based varistor usually contains a small amount of oxide additives, such as: Bi_2O_3, Sb_2O_3, CoO, and MnO [15].

I.5. Properties of zinc oxide Nanostructures:

I.5.1. Morphology Controlled:

Nanostructured materials are a class of materials having the dimensions in 1-100 nm range. This property provides the greatest potential applications because of the improved performance of the materials. ZnO provides a lot of variations of particles structures among all the known materials. ZnO can occur in 1-dimension (1-D), 2-dimension (2-D) and 3-dimension (3-D) forms. One dimensional nanostructure is more in number forming the largest group amongst all which includes nanorods, needles, rings, ribbons, tubes, belts, wires and combs. Zinc oxide can be obtained in 2D structures such as nanoplate, nanosheet, and nanopellets. There have also been many solution-based chemicals methods that involve the calcinations step as the final step for the synthesis of hierarchical porous ZnO micro-/nano- structures.

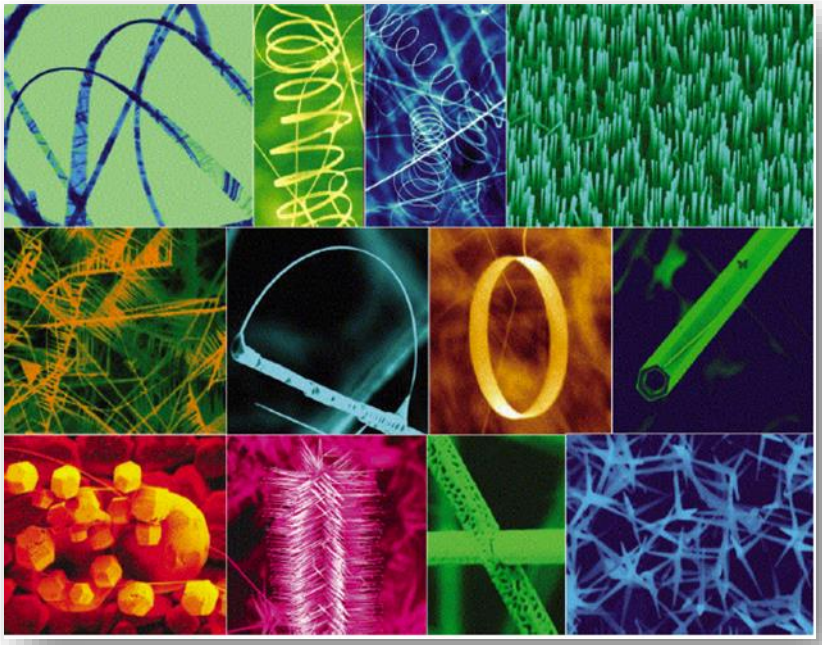

Figure I.7: Various ZnO nanostructures. Note: Scale bar is not shown [16].

I.5.2. Physico-chemical Properties:

As per the concept of quantum confinement, different morphology of structures leads to variation in their physical and chemical properties. Among various nanostructures, the belt, wire, and rod structures have been studied extensively from different sources. Below is a quick summary of each of them.

I.5.2.1. Nanobelts:

Nanobelt and some other relevant structures have their application in optoelectronics, optical and electrical devices like nanosensors and nanoactuators. With the reduction in object size, phonon densities and phonon modes of the states change drastically resulting in an unusual thermal transport phenomenon at the mesoscopic scale. Kulkarni et al. have measured the size-dependent thermal conductivity of zinc oxide nanobelts. The thermal conductivity of nanobelts is suppressed in comparison to that in the bulk due to increased phonon- boundary scattering and modified phonon dispersion. This size reduction affects any increase in localized heating but it has found potential application in the field of thermo-electronics.

I.5.2.2. Nanowires:

Li et al. have reported the electronic transport of ZnO nanowires. It was seen that the conductance decreased when the oxygen pressure was increased. This indicated that the surface oxygen species controlled the electric transport through each wire. Hence, it was helpful to demonstrate that the nanowires are useful to develop gas sensors that can work in ambient conditions. ZnO has also been recognized as an effective material in the blue UV region.

I.5.2.3. Nanorods:

ZnO nanorods have been proved to be useful in the detection of biological molecules. Kim and coworkers have functionalized ZnO nanorod's surface with biotin and have developed biosensors [16].

I.6. Advantages of zinc oxide:

The following are the most desirable characteristics of ZnO [17-20]:

- ZnO has an extremely large exciton binding energy of (60 meV) which is much greater than the thermal energy (26 meV) at room temperature. This is one of the key parameters that enable the UV laser diode and other exciton-related light-emitting devices to operate at room temperature.
- High transparency in the visible and near-infrared spectral region.
- ZnO is one of the "hardest" materials in II-VI compound semiconductors due to the higher melting point and larger cohesive energy. It can be expected that degradation of the material due to the generation of dislocations during the device operation will be reduced.
- Low material costs, nontoxicity, and abundance in the earth's crust.
- Interfacial energy between ZnO and sapphire or other oxide substrates is such that two-dimensional growth is favored, which results in high-quality films at a lower temperature.
- Possibility to prepare highly doped films with free electron density $n>10^{20}$ cm^{-1} and low resistivity ($<10^{-3}$ Ω cm).
- Good contact with the active semiconductors (absorber layers).
- Possibility to prepare the TCO layer on large areas (>1 m^2) by deposition methods like magnetron sputtering.
- Possibility to prepare ZnO films with suitable properties at low substrate temperature.

References:

[1] K. Ellmer, A. Klein, B. Rech. Transparent Conductive Zinc Oxide Basics and Applications in Thin Film Solar Cells, book published by Springer, (2008).

[2] Z. Yao. Doctorat Thesis, ZnO Nanoparticles as a Luminescent Down-Shifting Layer for Solar Cells, Ecole doctorale: Matériaux de Lyon, (2015).

[3] O. Behera. Doctorat Thesis, Synthesis and Characterization of ZnO Nanoparticles of Various Sizes and Applications in Biological Systems, Department of Computer Science and Engineering National Institute of Technology, Rourkela Rourkela-769 008, Orissa, India.

[4] A. Onodera and M. Takesada. Electronic Ferroelectricity in II-VI Semiconductor ZnO, in Advances in Ferroelectrics, Sapporo, Intech, p 231-225, (2013).

[5] Ü. Özgür, Ya. Alivov, C. Liu, A. Teke, M. A. Reshchikov, S. Doğan, V. Avrutin, S.-J. Cho, H. Morkoç. A Comprehensive Review of ZnO Materials and Devices, vol 98, p 1–103, (2005).

[6] J. Behler. A Neural Network Potential for Zinc Oxide, Available: http://www.theochem.ruhr-uni-bochum.de/~joerg.behler/zno.htm, (Accessed 16 February 2016).

[7] T. Hanada, T. Yao, S. Hong. Basic Properties of ZnO, GaN and Related Materials, in Oxide and Nitride Semiconductors; Processing, Properties and Applications, Heidelberg, Springer, p 1-19, (2009).

[8] B. K. Meyer, H. Alves, D. M. Hofmann, W. Kriegseis, D. Forster, F. Bertram, J. Christen, A. Hoffmann, M. Straßburg, M. Dworzak, U. Haboeck, A. V. Rodina. Bound exciton and donor-acceptor pair recombinations in ZnO, vol 241, p 231-260, (2004).

[9] A. Janotti and C. Van de Walle, C. Litton, D. Reynolds, T. Collins. Native Point Defects and Doping in ZnO, in Zinc Oxide Materials for electronic and optoelectronic device applications, Wiley, p 113-134, (2011).

[10] C. Van de Walle. Oxides as Semiconductors, Santa Barbara, (2014).

[11] C. Jagadish, S. Pearton. Zinc Oxide Bulk, Thin Films and Nanostructures: Processing, Properties and Applications, Amsterdam: Elsevier, (2006).

[12] J. Ungula. Growth And Characterization of ZnO Nanoparticles by sol-gel Process, QwaQwa, (2015).

[13] F. Bouaichi. Doctorat Thesis, Deposition And Analysis of Zinc Oxide Thin Films Elaborated Using Spray Pyrolysis for Photovoltaic Applications, University Mohamed Khider of Biskra, (2019).

[14] K. Manish. Doctorat Thesis, Zinc Oxide Nanostructures Synthesized by Oxidization of Zinc, Department of Metallurgical & Materials Engineering National Institute of Technology Rourkela, (2010).

[15] D. Dey, R.C. Bradt. Grain Growth in Sintering ZnO and ZnO–Bi2O3 Ceramics, Journal of the American Ceramic Society, vol 75, p 2529–2534, (1992).

[16] B. Ghata. Synthesis of Zinc Oxide Nanoparticles Through Various Methods, Its Characterization And Applications, University Gujarat Technological of Ahmedabad, (2017).

[17] C. Jin. Doctorat Thesis, Growth And Characterization of ZnO and ZnO-Based Alloys_MgxZn1-xO and MnxZn1-xO, University North Carolina State, (2003).

[18] K. Ellmer, A. Klein, K. Ellmer, A. Klein, B. Rech. Transparent Conductive Zinc Oxide Basics and Applications in Thin Film Solar Cells, book published by Springer, (2008).

[19] S. Shenlei, Doctorat Thesis, Exciton Related Optical Properties Of ZnO, University of Hong Kong, (2006).

[20] A. Khan. Doctorat Thesis, Synthesis Characterization And Luminescence Properties Of Zinc Oxide Nanostructures, University Ohio, (2006).

Chapter II : methods and materials

II.1. Introduction:

The second chapter is divided into two parts. The first part goes through the definition, different steps, advantages, and applications of the Sol-Gel process, then it describes the preparation steps of pure ZnO powders as well as the Bi-doped ones. The second part tackles the various characterization techniques utilized in this study.

II.2. Synthesis of Inorganic Nanomaterials:

Nanotechnology is a branch of material science in which nanoparticles with specific intended properties are synthesized or produced by the application of physical or chemical processes. The standard definition of a nanoparticle is a particle whose average dimensions are <100 nm.

Figure (II.1) presents different approaches to the synthesis of Inorganic Nanomaterials.

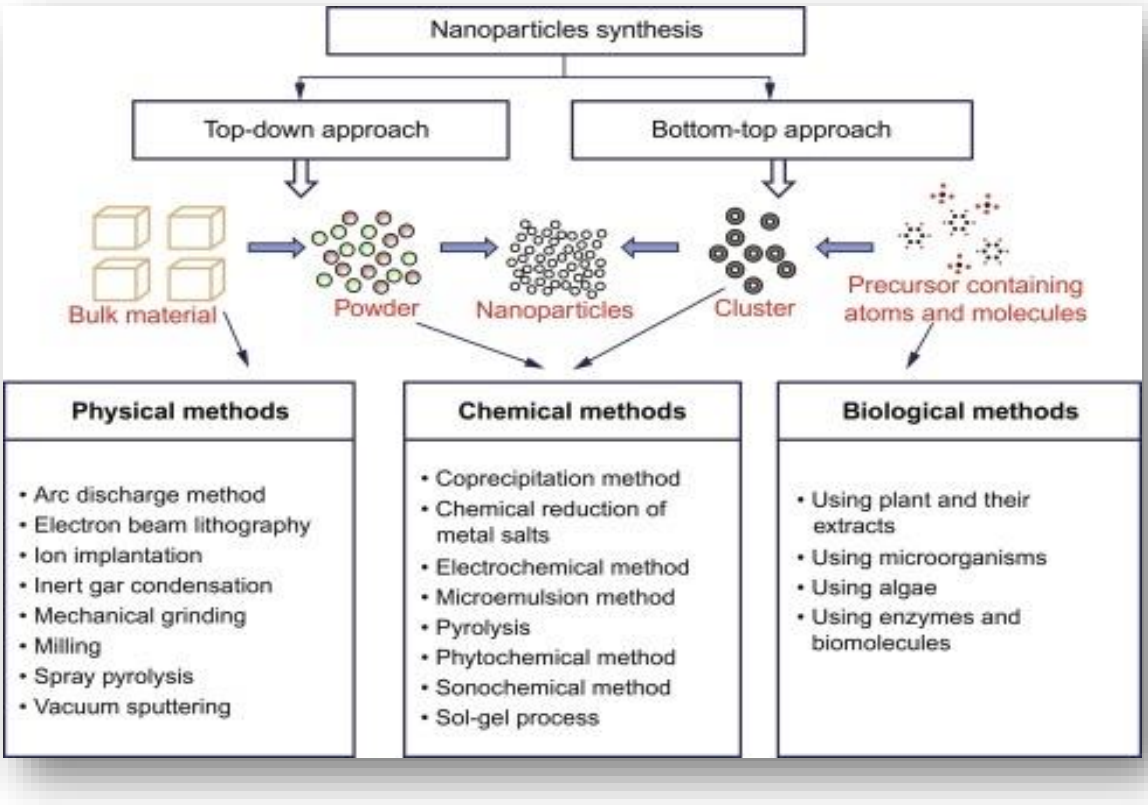

Figure II.1: Top-down and bottom-up approach for the synthesis of nanoparticles [1].

II.3. Sol-Gel process:

II.3.1. Introduction:

Sol-gel processing is a well-known, cost-competitive bottom-up synthesis approach used in material science and ceramic engineering to generate oxide nanopowder and composite nanoparticles from a sol followed by gel formation. Functionality refers to typical chemicophysical properties owned by materials [2].

II.3.2. An overview of sol-gel process steps:

The sol-gel process, as the name implies, involves the transition from a liquid 'sol' (colloidal solution) into a 'gel' phase [3]. Usually inorganic metal salts or metal-organic compounds such as metal alkoxideare used as precursors. A colloidal suspension or a 'sol' is formed after a series of hydrolysis and condensation reactions of the precursors. Then the sol particles condense into a continuous liquid phase (gel). With further drying and heat treatment, the 'gel' is converted into dense ceramic or glass materials. Generally, the reactions that are used to describe the sol-gel process are:

II.3.2.1. Hydrolysis and condensation:

- **Hydrolysis reaction:**

  During the hydrolysis reaction, the alkoxide groups (OR) are replaced with a hydroxyl group (OH) by adding water, as given in the equation below:

$$M(OR)_n + H_2O \rightarrow M(OR)_{n-1}(OH) + ROH \qquad \textbf{(II.1)}$$

  Although hydrolysis can occur without the use of an extra catalyst, it has been shown that the speed and extent of the hydrolysis reaction can be enhanced with the use of an acid or basic catalyst.

- **Condensation reaction:**

  The groups ($HO{-}M\ (-OR)_{n-1}$) generated during the hydrolysis react either with each other to give a molecule of water (oxolation) or with a molecule $\boldsymbol{M}$ of the alkoxy ($-OR$) to give an alcohol molecule (alcoxolation) and leading to the creation of the or each flight $\boldsymbol{MOM}$ oxygen atom becomes a bridge connecting two atoms of the metal $\boldsymbol{M}$. This leads to the formation of a gel whose viscosity

increases over time; this gel contains solvents and precursors which have not yet reacted.

II.3.2.2. Gelation:

The most basic description of gelation is that clusters increase via condensation of polymers or aggregation of particles until they collide, then links form between the clusters to produce a single enormous cluster known as a gel. This cluster reaches across the vessel that contains it, so the sol does not pour when the vessel is tipped. At the moment that the gel forms, many clusters will be present in the sol phase, entangled in; however, they are not attached to the spanning cluster. Over time, they progressively become connected to the network and the stiffness of the gel will increase.

II.3.2.3. Ageing:

After gelation, the continuing chemical and physical changes during ageing are extremely significant.

During this process, further cross-links continuous, the gel shrinks as the covalent links replace non-bonded contacts and both the pore sizes, and pore wall strengths change as the gel's structure evolves.

II.3.2.4. Drying:

Inside the structure, the gel contains a high water ratio and three-dimensional interconnected pores. Drying is necessarily required because the liquid trapped in the interconnected pores must be removed before the pore is closed during the densification process. On the other hand, removal of the liquid from the tiny pores causes significant stress resulting from inhomogeneous shrinkage. As a result, the main issue that needed to be solved was cracking owing to the large stress in the structure. For small cross-sections, such as: powder, coating, or fiber, the drying stress is small and can be accommodated by the materials, so no special care is needed to avoid cracking for those sol-gel structures. While for monolithic objects greater than 1 cm, drying stress developed in the ambient atmosphere can introduce catastrophic cracking, consequently, control of the chemistry of each processing step is crucial to prevent cracking during drying.

II.3.2.5. Densification:

Heat treatment of the porous gel at high temperature is necessary for the production of dense glass or ceramics from a gel. After the high temperature annealing, the pores are eliminated and the density of the sol-gel materials ultimately becomes equivalent to that of the fused glass. The densification temperature depends considerably on the dimension of the pores, the degree of connection of the pores, and the surface areas in the structure [4].

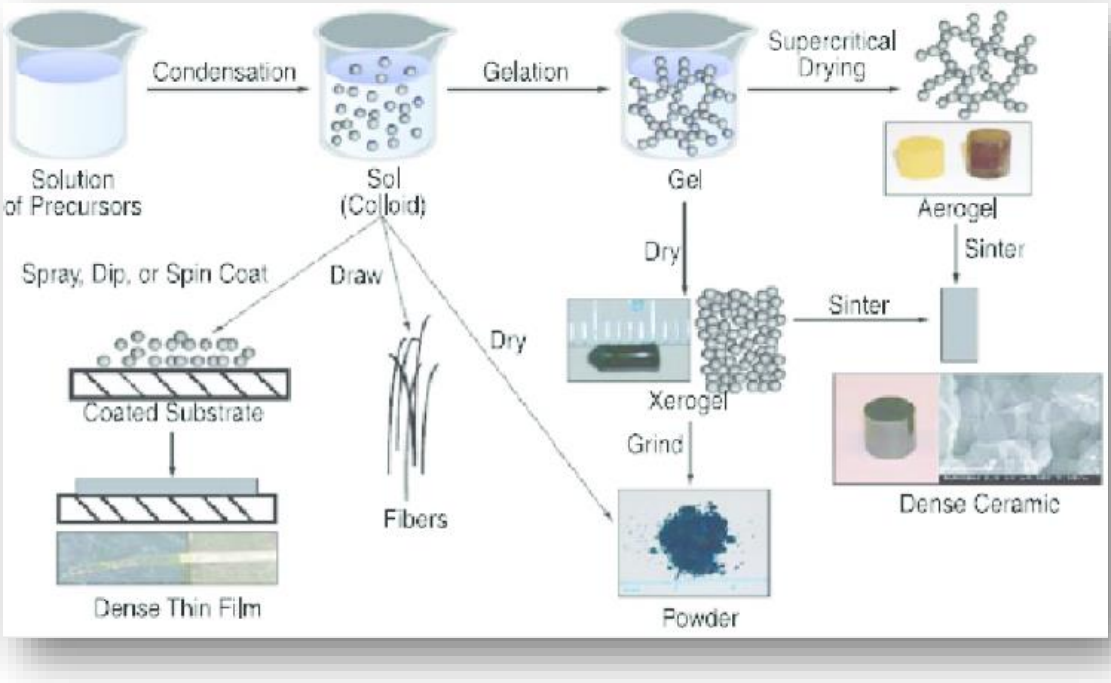

Figure II.2: Steps of the sol gel process of materials and examples of the microstructure of final products. Bold-lined rectangles show possible final products of the sol gel method [5].

II.3.3. Major control parameters of sol-gel process:

The macroscopic properties of the material are determined by its microstructure, and the microstructure is determined by the conditions of the material.

Generally speaking, the sintering properties of the powder vary in different preparation methods. While using large surface area and high surface activity of monodisperse ultrafine

ceramic powder, due to short diffusion distance and only need lower sintering temperature and activation energy.

Hydrolysis ratio, the acidity of the hydrolyzing agent, gelation condition, drying condition and procedures, and solvent types are all factors that influence the properties of final products obtained using the sol-gel technique.

II.3.3.1. Chemical compositions of the precursors:

The nature of the precursor can significantly affect the sol-gel reaction kinetics and final products.

II.3.3.2. Hydrolysis ratio:

The hydrolysis ratio, as defined by equation (II.2), is the main external parameter and has been shown to be important in controlling the hydrolysis and condensation of metal alkoxides [6]:

$$h = [H_2O]/[M(OR)_z] \quad \textbf{(II.2)}$$

where:

$[H_2O]$ and $[M(OR)_z]$ are the molar numbers for the water and metal alkoxide, respectively; $\boldsymbol{z}$ is the valance charge of metal $\boldsymbol{M}$.

The lower amount of water added is easy to form the product of low crosslinking, and the viscosity of the sol is increased; the higher amount of water added is easy to form a highly cross-linked product, and the viscosity is decreased. Therefore, the amount of water has an important effect on the structure of the product and the viscosity and gelation time. When h< 1, water molecules are not sufficient for complete hydrolysis, and thus gelation or precipitation cannot occur. When 1<h <z, chainoxypolymers can form. When h >z, cross-linked oxypolymers can be obtained and nanoparticles or gels can be formed. The hydrolysis ratio also has a great influence on the hydrolysis and condensation rate. When h is low (< ~1), the hydrolysis rate is low, so the sol-gel reaction rate including hydrolysis and condensation is also slow. When h is high (< ~7), the hydrolysis rate is high, but the condensation rate is low, the result being a slow sol-gel reaction. When h is intermediate (1< h < 7), the sol-gel reaction is the fastest because of high rates of both hydrolysis and condensation [7].

II.3.3.3. Catalysts:

Both acids and bases can catalyze sol-gel reactions. The hydrolysis and condensation reactions can be explained by SN2 nucleophilic substitution reaction mechanism. Take alcohol as an example, it is not easy to hydrolyze silicon alkoxide and its hydrolysis; polymerization are usually catalyzed by acid or alkali. The inorganic acid can make the partially negatively charged alkoxy matrix so that it is easy to break away from the silicon atom. Alkali provides nucleophilic hydroxyl OH in alkali-catalyzed hydrolysis, and Si-OH loss of protons, thereby accelerating polymerization. In the presence of excess water, because of the acid-catalyzed hydrolysis reaction, Si (OH) can be formed. The rate of polymerization is faster than that of hydrolysis under the condition of alkali catalysis. Acid or base catalysis is not the only catalyst. Some nucleophiles, as: NaF or 2-methylpyridine, also have the ability to improve the reaction rate.

II.3.3.4. pH value:

Zinc oxide (ZnO) nanoparticles were prepared and synthesized via the sol-gel method, using citric acid as a precursor. The annealing temperature was fixed at 600 °C. The impact of pH on particle size was investigated. Three different pH (3.0, 5.0, and 1.01) for the precursor were chosen, and it was revealed that the Zn NPs size increased with the alkalinity of the precursor. The pH value of the sol-gel solution will change when added with acids and alkalis to catalyze the reactions. Experimental results indicate that the pH value and hydrolysis ratio have a synergistic effect on the morphologies of the products [8].

II.3.3.5. Reaction temperature:

Generally, increasing temperature results in both hydrolysis and condensation rate increase [7, 9].

II.3.4. Advantages and shortages of sol-gel processing:

The sol-gel process provides samples with high purity, homogeneity, and structure of easy control. The most important advantages of the sol-gel process in the preparation of functional materials are as follows [2]:

- In all stages, the temperatures required are low and close to room temperature. Then, thermal decomposition of organic material and any entrapped species is minimized leading to high purity and stoichiometry.

- As the organometallic precursors for different metals are miscible, the homogeneous sol solutions are easily achieved. Since the sol-gel is initiated by the reaction of the solution, the materials are very uniform and easy to modify, which is crucial for controlling the physical and chemical properties of the material.
- Precursors such as metal alkoxides and mixed alkyl/alkoxides are easily purified by common techniques (e.g. distillation or sublimation), which lead to high-purity products.
- The chemical conditions are mild in sol-gel process. Hydrolysis and condensation are catalyzed by acid or alkali under mild pH conditions.
- Highly porous and nanocrystalline materials can be synthesized by this method.
- Colloid particle size and pore size, porosity, and chemistry of the final product can be optimized by chemical treatment of the precursors, controlled rates of hydrolysis, and by condensation.
- Incorporating several components in a single step or in two steps.
- Production of samples in different physical forms. Starting from the same raw material, changing the process can get different products, such as fiber, powder, or film and composite materials.
- Treating temperature is low, the inorganic materials can be synthesized under the condition of low temperature at about 600 °C, the composition and the structure of the product are uniform, the grain size is small, the activity of the material particles is increased, and the performance of the material is expanded.
- Suitable for large-scale industrial production.

The disadvantages of sol-gel processing include high precursor cost, overall high cost, and environmental problems associated with the disposal of large quantities of organic by-products. A common theme out of the negative comments was wet chemical processing using alkoxides as precursors [10].

The sol-gel process is more complex in terms of the difficulty in phase control, which is the different chemical and crystal morphology formation at different temperatures. The morphology is relatively simple, generally, and spherical particles.

Gelation, drying, and heat treatment take much time to prepare the sample. In the drying and heat treatment stage, the sample has a great weight loss and residual stress; film

prone to cracking and objectively restricting the thickness of thin film and result in film residual porosity.

II.3.5. Applications of Sol Gel method:

The sol-gel technology is highly efficient in producing various factional materials, and successful applications have been achieved which can be summarized in a scheme (Figure II.3) where examples of applied materials in electronics, optics, photonics, high-temperature technologies, chemical technologies, biochemistry, and medicine are given.

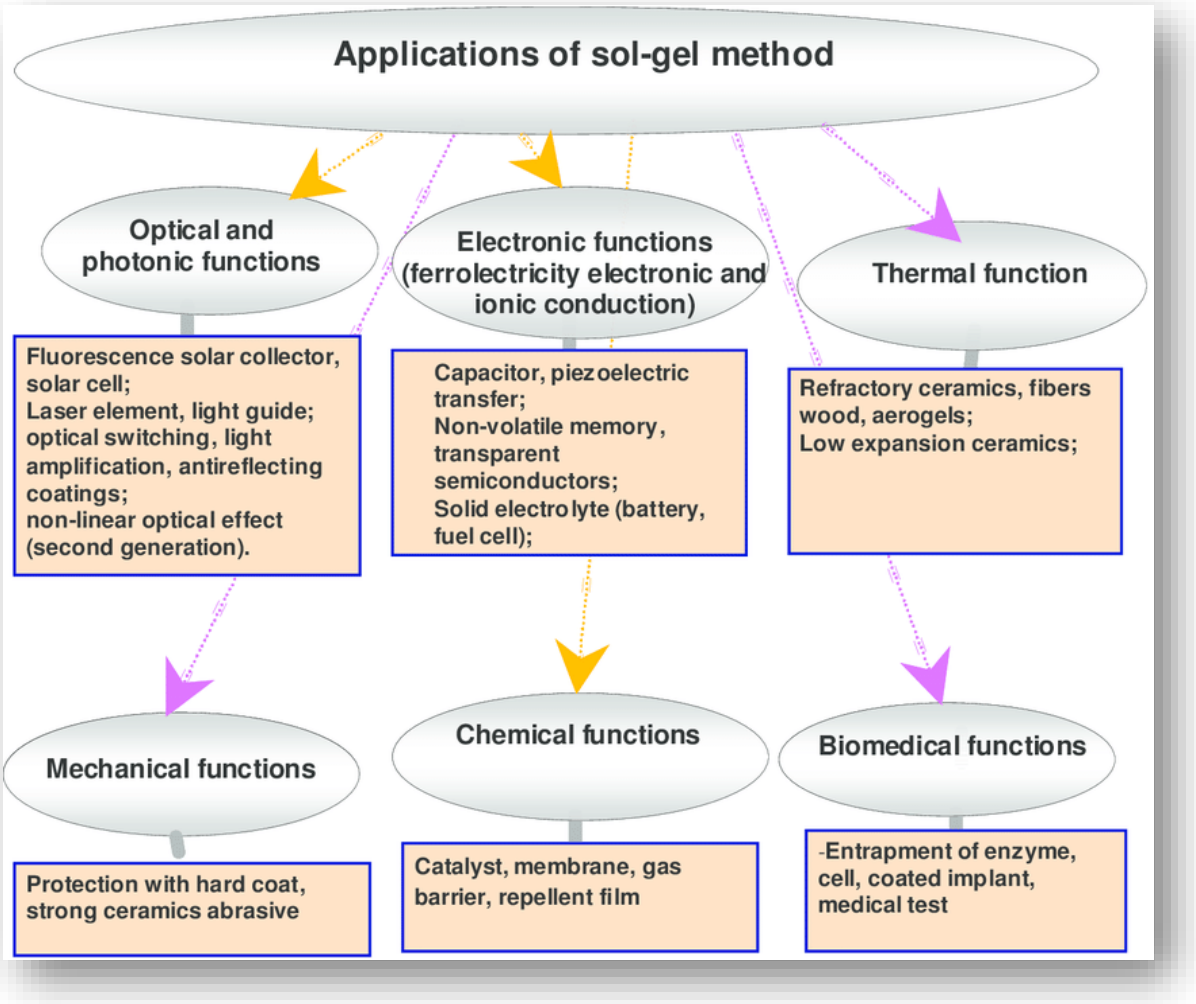

Figure II.3: Applications of sol gel method [11].

II.4. Synthesis of pure and Bi doped zinc oxide powder:

The synthesis of pure and Bi-doped zinc oxide nanoparticles using the sol-gel method was carried out using the following material:

- **Zinc acetate dihydrate ($C_4H_6O_4Zn.2H_2O$)**: used as a starting material.
- **Citric acid ($C_6\ H_8O_7$)**: An alkoxide, used to keep particles in suspension.
- **Ethylene glycol ($C_2H_6O_2$)**: used as a solvent.
- **Bismuth (III) nitrate (Bi $(NO_3)_3$)**: used as a dopant.

The following table (II.1) represents some proprieties of the different precursors we used:

Table II.1: the physical and chemical properties of different chemicals used in this work [12].

Chemical compound	Formula	Molar mass(g/mol)	Melting point(°C)	Appearance	Density (g/cm3)
Zinc acetate dihydrate	$C_4H_6O_4Zn.2H_2O$	219.51	237	White solid (all forms)	1.84
citric acid	$C_6\ H_8O_7$	192.124	153	white solid	1.66
ethylene glycol	$C_2H_6O_2$	62.07	-13	Clear,colorless liquid	1.28
Bismuth(III) nitrate [13]	Bi(NO3)3.5H2O	485.07	33	colorless, white	2.83

II.4.1. Experimental conditions:

Controlling the experimental conditions is compulsory for the preparation of nanopowders, important parameters are :

- The concentration of the chemical precursors.
- The temperature of the bath.
- The duration of the gel formation.
- The temperature of the calcination 500 °C.
- The duration of the calcination.

II.4.2. Experimental details:

II.4.2.1. Pure ZnO nano-powders:

Pure ZnO nanoparticles have been synthesized using the sol-gel method starting with two solutions. The first solution was prepared by dissolving zinc acetate (C4H6O4Zn_2H2O) (with the concentration C_1=0.15 mol/l) in ethylene glycol. The second one was set by dissolving citric acid (with the concentration C_2=2.5 mol/l) in ethylene glycol too. Both of the solutions were placed in a bath of paraffin oil; heated at a well-fixed temperature. To maintain this homogeneous and fixed temperature a hot plate magnetic stirrer was used**.** After the complete dissolution of the precursors and the stabilization of the oil bath temperature, the two solutions were mixed. The first one was gradually added to the second with a molar ratio (C_1/C_2=0.06). Then, the obtained solution was stirred at 130 °C for 6h to obtain a homogeneous and transparent solution. Finally, the solution was calcined at 500 °C for 4h.

II.4.2.2. Bi-doped ZnO nano-powders:

Bismuth oxide is an excellent material for optoelectronic applications. It possesses nonlinear optical properties. Its high photoconductivity, large gap, and its dielectric permittivity make it an interesting and much-studied material [13].

The same steps for the undoped ZnO (pure ZnO) preparation were followed for the preparation of Bi-doped Zno. Zinc acetate was dissolved in ethylene glycol with the addition of the bismuth source: Bismuth (III) nitrate with an appropriate amount to obtain the desired concentrations (3 to 8 % Bi).

The following picture shows the obtained powder.

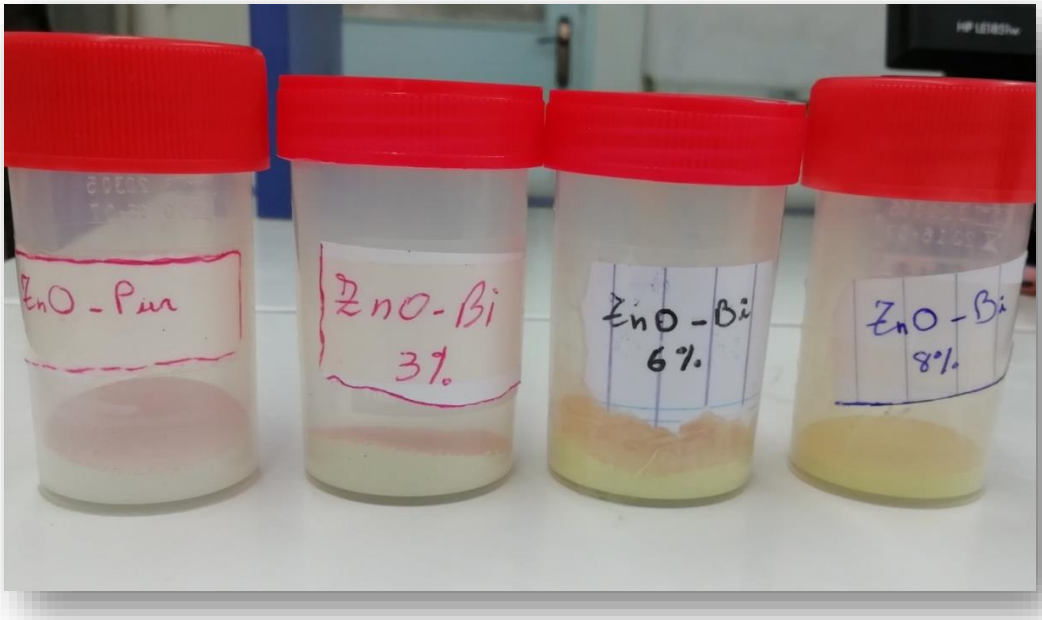

Figure II.4: Pure and Bi-doped ZnO powders.

Table (II.2) presents the experimental conditions for the preparation of pure and doped ZnO powders. The choice of these parameters is based on previous studies [12].

Table II.2: Experimental conditions for the production of pure and Bi-doped ZnO nanopowders.

Percentage of the dopant Bi (%)	Concentration C_1 (ZA) (mol/l)	Concentration C_2 (CA) (mol/l)	Concentration ratio C_1/C_2	Gelation temperature Tg (°C)	Gel time tg (h)	Calcination temperature Tc (°C)
0	0.15	2.5	0.06	130	6	500

The same conditions were followed for all the doping concentrations.

II.4.3. Calcination treatment:

Calcination is an operation that consists of transforming the gel into a powder. The thermal cycle was composed of a single step of 4hours at 500 °C with a rate of 5 °C/min.

Figure (II.5) indicates the oven we used for the calcination.

Figure II.5: Nabertherm oven.

The flowchart figure (II.6) summarizes the steps that took place in the powder preparation:

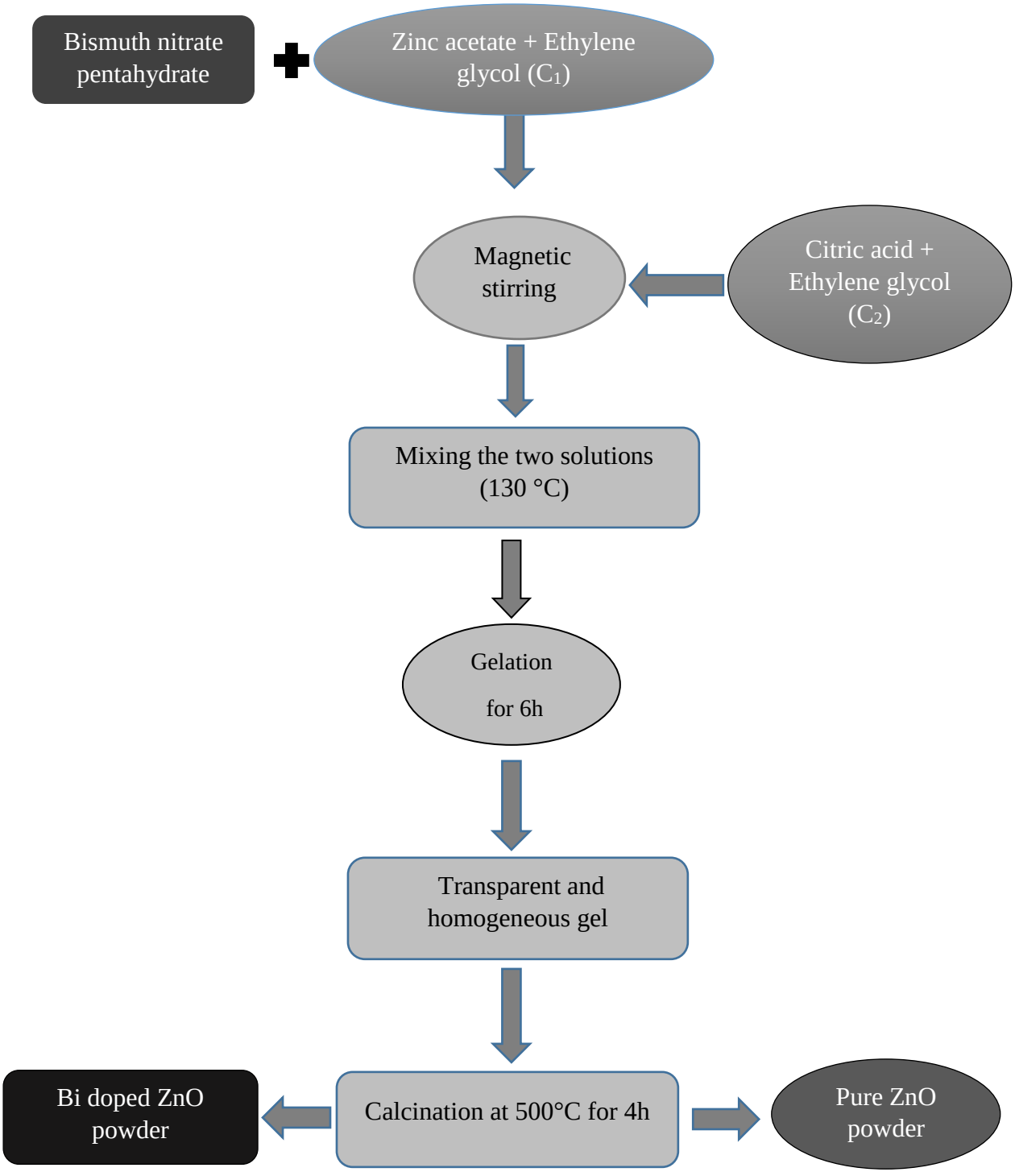

Figure II.6: flowchart of the synthesis of pure and Bi doped ZnO nanopowders using sol gel method.

II.5. ZnO powder characterization techniques:

II.5.1. Structural characterization:

For the structural characterization, we made the recording diagrams of X-ray diffraction (XRD) of the four obtained samples.

II.5.1.1. X-ray diffraction (XRD):

X-ray diffraction is a non-destructive structural analysis method for determining the crystal structure of materials in the form of bulk materials, powders, or thin films. It is based on the Bragg law (Figure II.7) which gives the relation between the distance $\mathbf{d_{hkl}}$ between the crystallographic planes, the wavelength **λ** of the X-rays, and the diffraction angle **θ**:

$$2d_{hkl}.\sin\theta = n\,\lambda \qquad \textbf{(II.3)}$$

Where:

$\mathbf{d_{hkl}}$: the interplanar distance, **θ**: X-ray incidence angle, **n**: the order of diffraction, **λ**: the wavelength of X-rays.

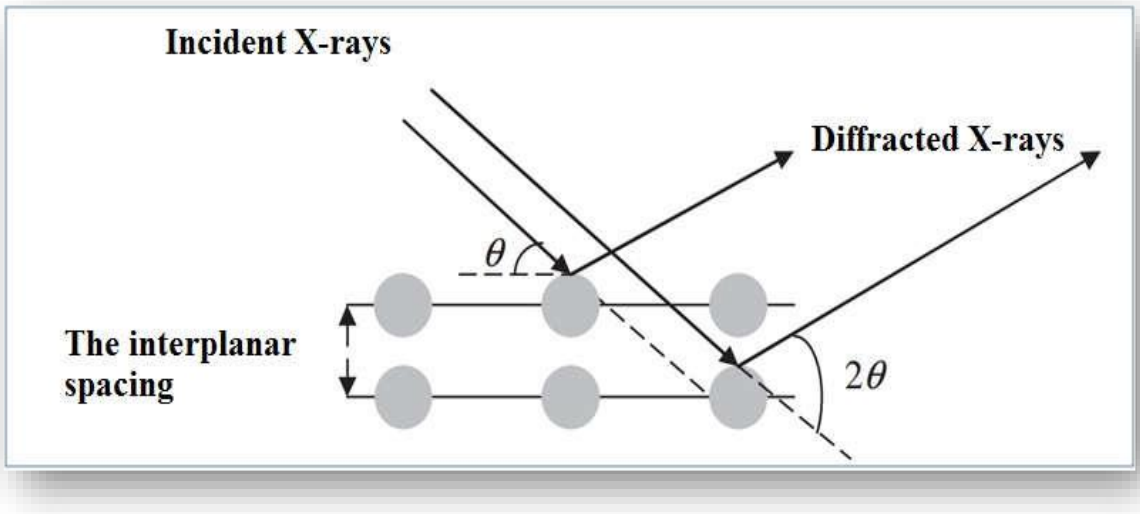

Figure II.7: The Principle of Bragg's Law [14].

II.5.1.2. Determination of the grains size:

The average crystallite size ***D*** can be estimated from the broadened peaks by using the Debye-Scherrerequation which is given by:

$$D = \frac{0.9\,\lambda}{\beta\,cos\theta} \qquad \textbf{(II.4)}$$

Where:

β is the full width at half maximum of a diffraction line located at angle **θ** while **λ** is the X-Ray diffraction wavelength. In this study, the XRD measurements were made using The **Rigaku *MiniFlex 600*** diffractometer.

Figure II.8: **The Rigaku MiniFlex 600 diffractometer.**

Figure (II.9) shows the schematic diagram of the XRD system.

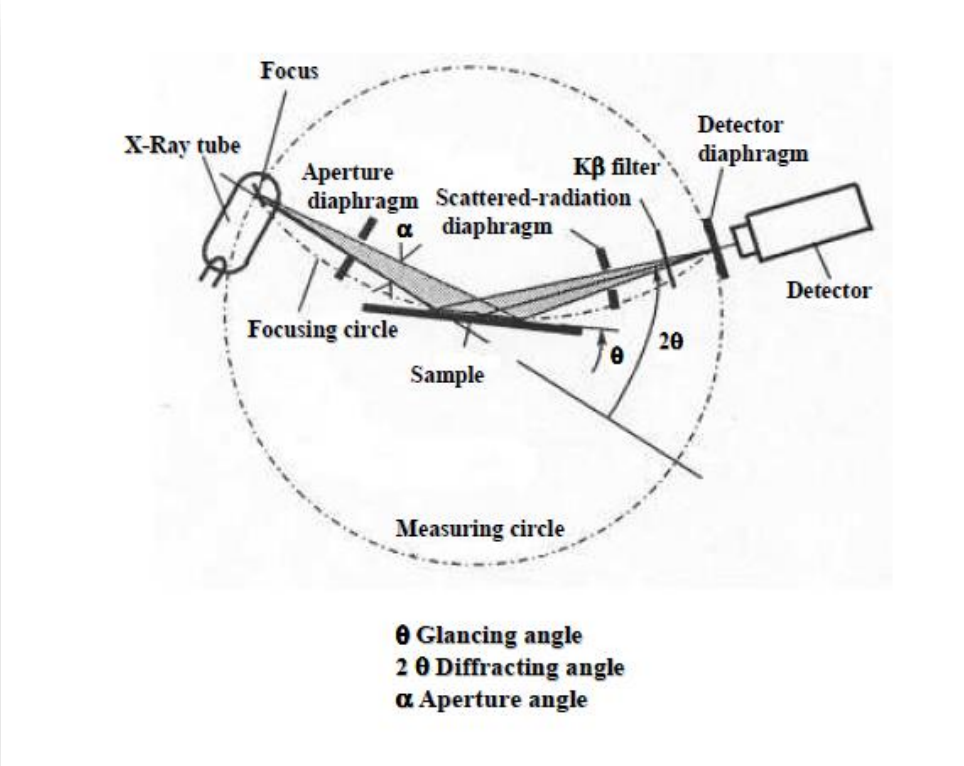

Figure II.9: Schematic of the system for XRD measurements [15].

II.5.1.3. Determination of the interreticular distances and the cell parameters:

The lattice parameter values for the Hexagonal systems can be calculated from the following equation using the (hkl) parameters and the interplanar spacing **d** [16].

$$\frac{1}{d^2} = \frac{4}{3}\left(\frac{h^2+hk+k^2}{a^2}\right) + \frac{l^2}{c^2} \qquad \textbf{(II.5)}$$

Where:

a, c = the cell parameters, ***h, k, l***= Miller's indices.

II.5.1.4. Determination of the lattice strain and the dislocation density:

The origin of micro strain **ε** is calculated using the relation [17]:

$$\varepsilon = \frac{\beta \cos\theta}{4} \qquad \textbf{(II.6)}$$

The dislocation density **δ** is the dislocation lines per unit area of the crystal can also be evaluated from the crystallite size **D** using the formula [18]:

$$\delta = \frac{1}{D^2} \quad \textbf{(II.7)}$$

II.5.1.5. Determination of texturing coefficients:

To determine the texturing coefficients we used the following relationship [19]:

$$TC_{hkl} = \frac{I(hkl)/I_S(hkl)}{n^{-1}\sum_n I(hkl)/I_S(hkl)} \quad \textbf{(II.8)}$$

Where:

TC_{hkl} is texture coefficient, **I (hkl)** is the measured XRD intensity of a plane (hkl), **I_s (hkl)** is the standard intensity of the plane (hkl), and **n** is the number of diffraction peaks considered.

II.5.2. Optical characterization:

UV-Visible spectrophotometry is based on the interaction of electromagnetic radiation and matter in the following spectral domains: Ultraviolet-Visible and Infrared. We can obtain certain optical properties of our samples using this technique, such as the curve of transmittance or absorbance versus UV-visible spectrum wavelengths, the determination of the band gap energy (Eg), the optical absorption threshold, the absorption coefficient, the refractive index, and the extinction coefficient [20].

Figure (II.10) shows UV-Visible spectrophotometer.

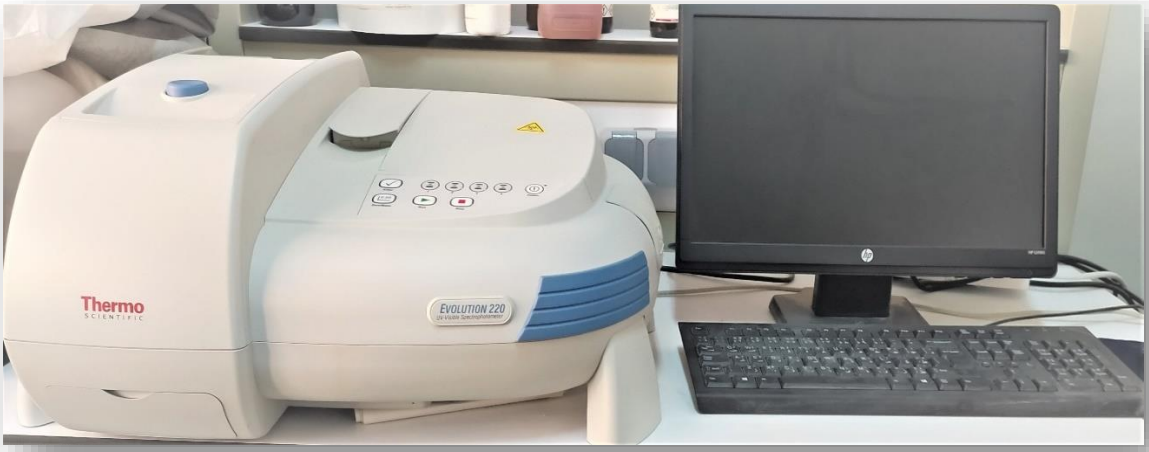

Figure II.10: EVOLUTION 220 spectrophotometer image.

II.5.2.1. The Optical Gap:

From the transmittance spectrum in the UV-visible, one can quickly determine the optical gap. Electronic transitions between wide states of band to band cause absorption at high energies. Tauc law is generally used to describe it:

$$(\alpha h\nu) = A\,(h\nu - Eg)^{m} \qquad \textbf{(II.9)}$$

Where:

hν is the photon energy, ***Eg*** is optical gap **m** and **A** are constants. ***m*** characterizes the optical type of transition and takes the values ½ for allowed direct transitions or 2 for allowed indirect transitions.

To identify the nature of the transition from the powders that are produced in this study, we will plot the curves $(\alpha h\nu)^2 = f(h\nu)$ and by extrapolation to $(\alpha h\nu)^2 = 0$ one can get **Eg** value as shown in (Figure II.11):

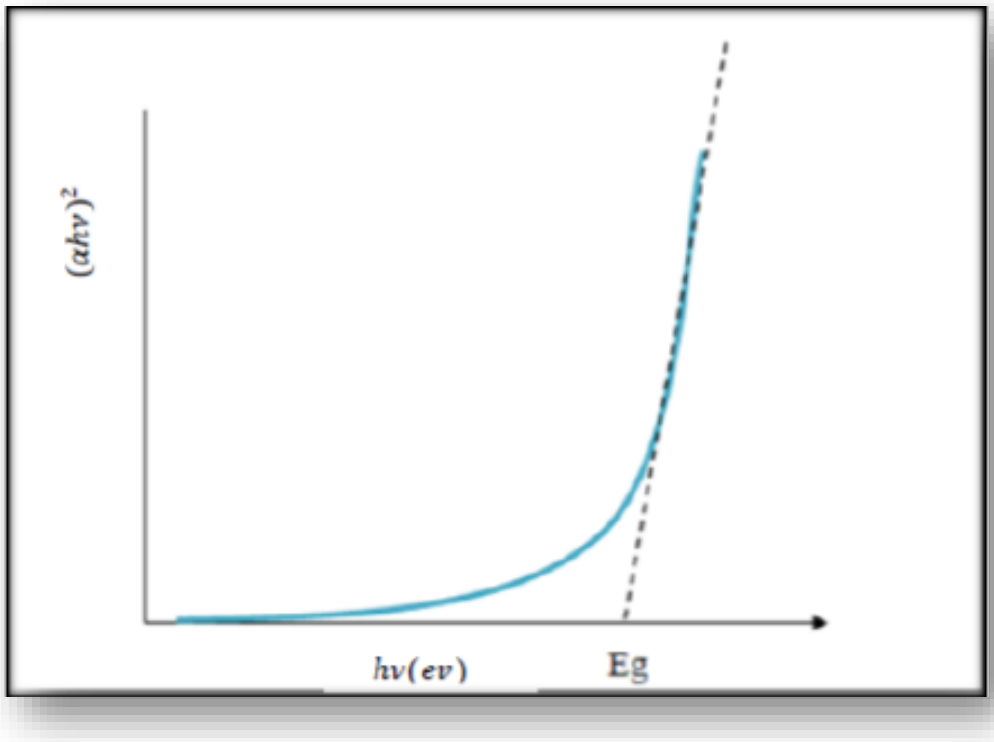

Figure II.11: determination of Eg [21].

II.5.2.2. The Absorption Coefficient:

We can determine the absorption coefficient for each value of transmittance **T** in (%) which corresponds to energy by the law of Beer-Lambert [21].

$$T = \frac{I}{I_0} * 100 \qquad \textbf{(II.10)}$$

Where:

$$\frac{I}{I_0} = exp - \alpha d = \frac{T}{100} \qquad \textbf{(II.11)}$$

I_0 is the incidental light intensity, **I** the transmitted light intensity, **α** coefficient of absorption and **d** the thickness of the cell. This relation can be written:

$$\alpha = \frac{1}{d} ln(\frac{I_0}{I}) \qquad \textbf{(II.12)}$$

If we express ***T (λ)*** in (%), the previous expression becomes:

$$\alpha = \frac{1}{d} ln(\frac{100}{T}) \quad \textbf{(II.13)}$$

II.5.2.3. Urbach energy:

Another important parameter, which characterizes the material disorder, is Urbach energy. Ac-cording to the Urbach law of the expression of the absorption coefficient is as follow [22]:

$$\alpha = \alpha_0 \exp(h\nu/E_{00}) \quad \textbf{(II.14)}$$

By drawing the **ln(α)** on function of ***hν***, one can determinate $\mathbf{E_{00}}$value:

$$\ln\alpha = \ln\alpha_0 + (h\upsilon/E_{00}) \quad \textbf{(II.15)}$$

The following (Figure II.12) presents how we can estimate E_{00}

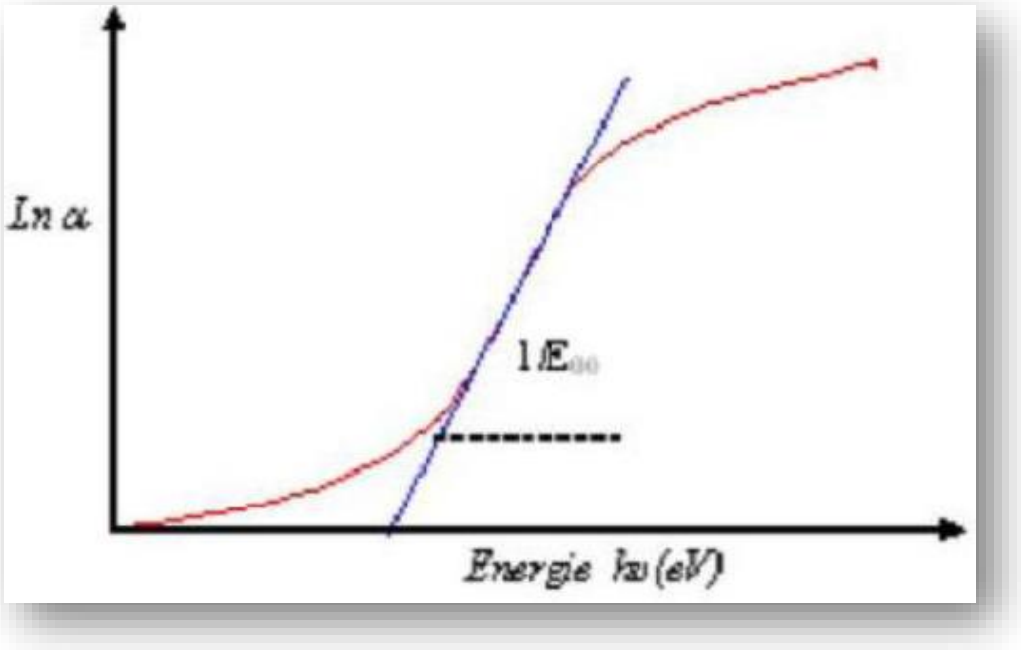

Figure II.12: Determination of the disorder by extrapolation starting from the variation of Ln (α) as in function of hν [23].

II.5.2.4. Sample preparation:

A small amount of ZnO powder was measured and then dissolved in the solvent of choice (Hydrochloric acid 37%). The cell was then filled with 3.5mL of the solution (ZnO+Hydrochloric acid 37%) and wiped before putting it into the spectrometer.

II.5.3. Chemical characterization:

Vibrational spectroscopies (Infrared Spectroscopy (IR)) probe the vibrations of atoms in molecules or solids so as to identify the chemical compositions of the sample. The crystalline structure can also be analyzed from vibrational spectroscopies to a certain extent. The IR spectroscopy measures the absorption spectrum of photons directly.

II.5.3.1. Fourier Transform Infrared Spectroscopy (FTIR):

Each chemical bond, in solids or molecules, has specific (quantized) vibrational modes. These modes, acting as oscillators, can absorb photons of energy corresponding to the oscillator transition. The absorption spectrum is thus “a picture” of the chemical bonds present in the sample, provided that they are IR active, i.e. having a dipole moment, capable of absorbing the electromagnetic radiation.

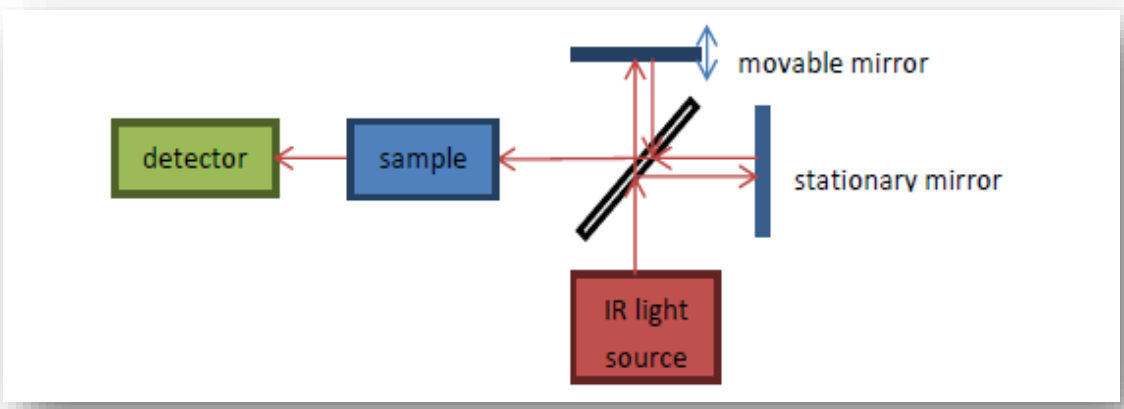

Figure II.13: Schematic diagram of the operational principle of the Michelson interferometer [24].

IR absorption spectroscopy can be performed using either a monochromatic source or a broad spectrum IR source. Before the incident light arrives at the sample, it is divided by a beam splitter into two light beams and reflected by a stationary and a movable mirror, respectively. The two reflected light beams then recombine and undergo interference which is normally called the Michelson interferometer, as shown in (Figure II.13). The recombined light illuminates the studied samples, and the transmitted or deflected light is detected. The transmittance spectrum can be obtained from the collected signal and the interferogram is treated by the Fourier transform. The absorption spectrum can also be converted from the transmittance spectrum using programs integrated in the FTIR instrument.

The method using the broad band IR source has the advantage of being faster and more sensitive than the simpler one using a monochromatic source.

A common Fourier Transform Infrared Spectroscopy (FTIR) is able to cover a long range of electromagnetic spectrum regions [24]:

The near-infrared (0.8–2.5 μm), mid-infrared (2.5–25 μm) and far infrared (25–1000 μm).

II.5.3.2. Sample preparation:

The sample is prepared by grinding a quantity of zinc oxide powder with a mass of (m=0.001 g) with a specially pure salt (Potassium bromide (KBr)) with a mass of (0.2 g) for the mixture to become homogeneous, then it is pressed at 5.5 tons to obtain transparent granules through which a bundle can pass via Spectrophotometer.

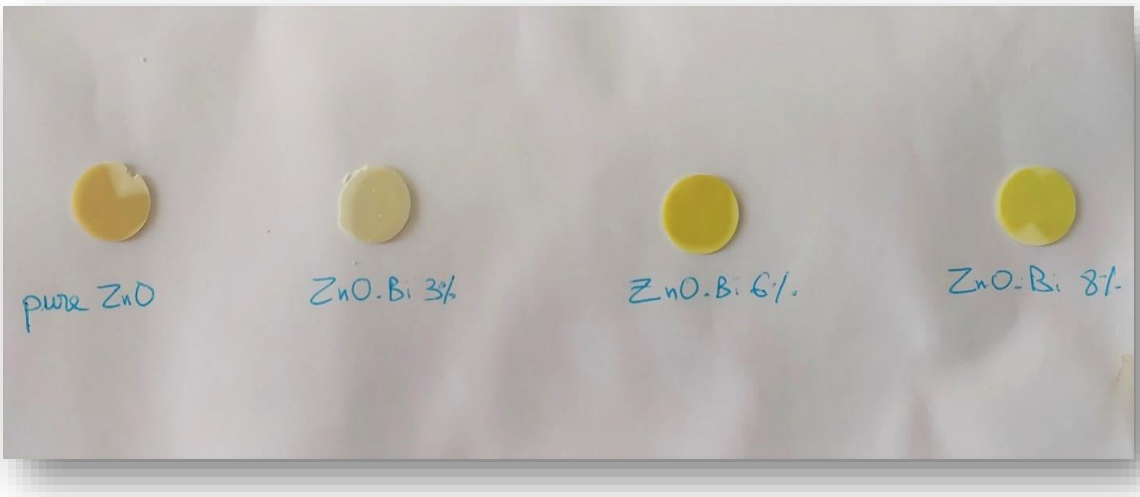

Figure II.14: Transparent granules of pure and doped zinc oxide.

References:

[1] C. P. Devatha, A. K. Thalla. Green Synthesis of Nanomaterials. Elsevier Ltd, (2018).

[2] S. Amiri, A. Rahimi. Hybrid Nanocomposite Coating by sol–gel Method: A review, Iranian Polymer Journal, (2016).

[3] J. D. Wright, N. A. J. M. Sommerdijk. Sol-gel Materials: Chemistry and Applications. Advanced Chemistry Texts, Gordon and Breach Science Publishers, (2001).

[4] M. Dahnoun. Doctorat Thesis, Preparation and haracterization of Titanium dioxide and Zinc oxide thin films via Sol-Gel (spin coating) technique for optoelectronic applications, University Mohamed Khider of Biskra, (2020).

[5] A. Chládová, J. Wiener, J. M. Luthuli, V. Zajícová. Dyeing of glass fibres by the sol gel method, vol 11, no 1, p 18–23, (2011).

[6] VG. Kessler, GI. Spijksma, GA. Seisenbaeva, S. Hakansson, DHA. Blank, HJM. Bouwmeester. New insight in the role of modifying ligands in the sol–gel processing of metal alkoxide precursors: A possibility to approach new classes of materials, Journal of Sol-Gel Science and Technology, vol 40, p 163-179, (2006).

[7] C. Liu, L, Shaw. Nanoparticulate materials and core/shell structures derived from wet chemistry methods. In: Bharat Bhushan, Editors. Encyclopedia of Nanotechnology, Dordrecht: Springer Netherlands, p 1-21, (2015).

[8] K. Lee, BH. Guan, HM. Zaid, H. Soleimani, DLC. Ching. Impact of pH on zinc oxide particle size by using sol-gel process. In: 4th International Conference on Fundamental and Applied Sciences, p 1787, (2016).

[9] J. Livage, M. Henry, C. Sanchez. Sol–gel chemistry of transition metal oxides. Progress in Solid State Chemistry, vol 18, p 259-341, (1988).

[10] DR. Uhlmann. The future of sol-gel science and technology, Journal of Sol-Gel Science and Technology, vol 8, p 1083-1091, (1997).

[11] N. Khan. History of science and technology, vol 21, no 6, p 510, (2001).

[12] L. Arab. Thèse de Doctorat, Elaboration par différentes méthodes et étude optique de pouders nanocristallines de ZnO pur et dopé par différents oxyde, Université Mohamed Khider Biskra, (2012).

[13] T. Ait ahcene. thèse de Doctorat, Elaboration, Etude nanostructurale et proprietes electriques de nanomateriaux du systeme ZnO - Bi2O3, Université Mentouri de Constantine, (2007).

[14] Y. Liu. Thèse de Doctorat, Caractérisation de couches minces de ZnO élaborées par la pulvérisation cathodique en continu , Université du Littoral côte d'Opale, (2012).

[15] J. R. Connolly. Introduction to X-Ray Powder Diffraction, Springer, (2007).

[16] A. Aldrin. Doctorat Thesis, Preparation and characterization of certain II-VI, I-III-VI2 semiconductor thin films and transparent conducting oxides, Cochin University of Science and Technology, Kerala, India, (2004).

[17] Y. Zhao, J. Zhang. Microstrain and grain-size analysis from diffraction peak width and graphical derivation of high-pressure thermomechanics, vol 41, p 1095–1108, (2008).

[18] F. Szekely, I. Groma, J. Lendvai. Characterization of self-similar dislocation structures by X-ray diffraction, Mater, vol 324, p 179–182, (2002).

[19] S.Ilicana, Y. Caglara, M. Caglara, F.Yakuphanoglu. Electrical Conductivity, Optical and Structural Properties of Indium-Doped ZnO Nanofiber Thin Film Deposited by Spray Pyrolysis Method. Physica E , vol 35, p 131-138, (2006).

[20] N. Abdeouahab. Doctorat Thesis, Preparation and characterization of thin films nanostructures based on ZnO and other oxides, (2019).

[21] A. Hafdallah. Thesis Magister, Étude Du Dopage Des Couches Minces De Zno Élaborées Par Spray Ultraso- Nique, University Mentouri Constantine, (2007).

[22] F. Zhu, K. Zhang, E. Guenther, Ch.S. Jin. Optimized Indium Tin Oxide Contact For Organic Light Emitting Diode Applications, Institute Of Materials Research & Engineering, Singapor, (2000).

[23] K. Daoudi. Thèse de Doctorat, Elaboration Et Caractérisation De Films Minces D'oxyde D'indium Dope A L'etain Ob-Tenus Par Voie Sol-Gel, Potentialité Pour La Réalisation D'électrodes Sur Silicium Poreux, University Claude Bernard Lyon 1, (2002).

[24] Z. Yao. ZnO Nanoparticles as a Luminescent Down-Shifting Layer for Solar Cells, Materials. INSA de. Lyon, (2015**)**.

Chapter III : results and discussions

III.1. Introduction:

The current chapter presents and discusses the results that have been obtained for pure and doped ZnO nano-powders. We have used bismuth (Bi) as a doping agent and we have studied the main structural and optical properties of zinc oxide nanopowders as a function of bismuth doping concentration in order to investigate the influence of this doping rate on zinc oxide powders properties.

III.2. Results and discussions:

III.2.1. Structural study:

Powder X-ray diffraction (XRD) data were carried out with a Mini-Flex (Rigaku) diffractometer with a copper anode having a wavelength $\lambda_{k\alpha}$ (Cu) = 1.5405Å. The samples were scanned from 20° to 80° (2θ). XRD patterns of pure and Bi-doped ZnO powders with different doping concentrations (3%, 6%, and 8%) are reported respectively in (Figures III.(1-4)).

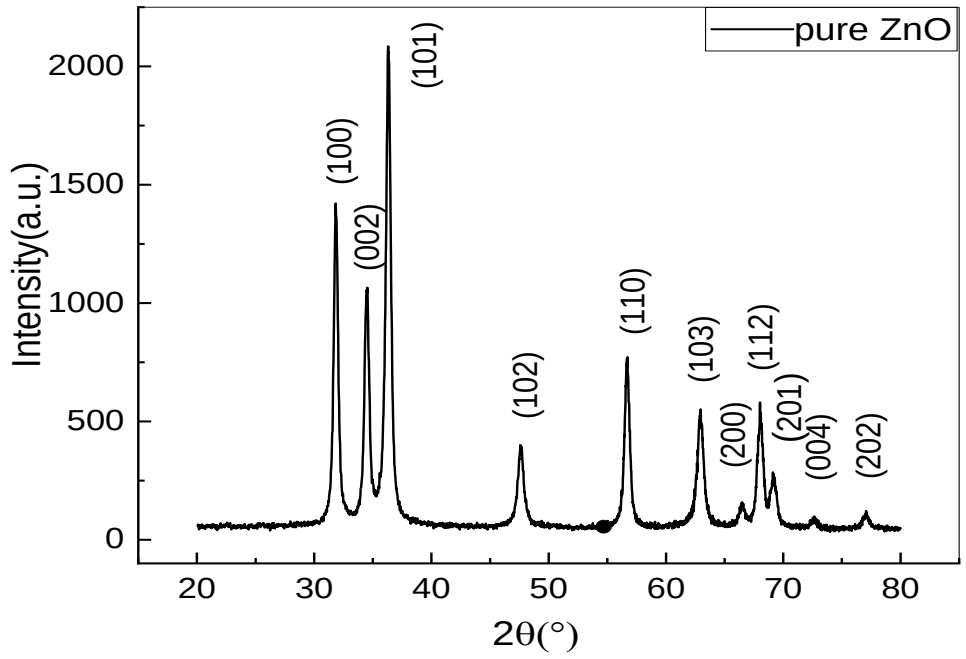

Figure III.1: XRD pattern of undoped ZnO powders.

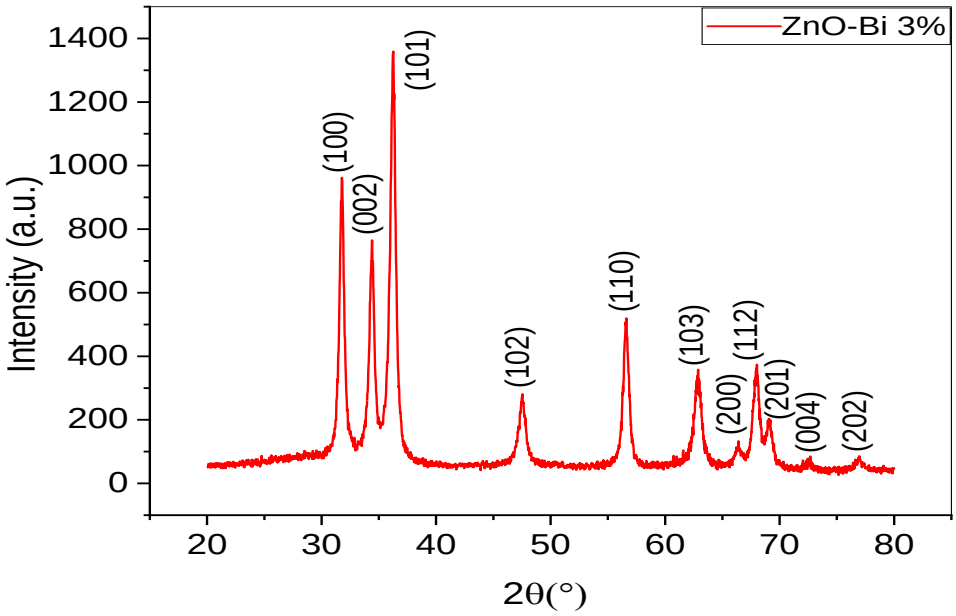

Figure III.2: XRD pattern of Bi-doped ZnO with a doping concentration of 3%.

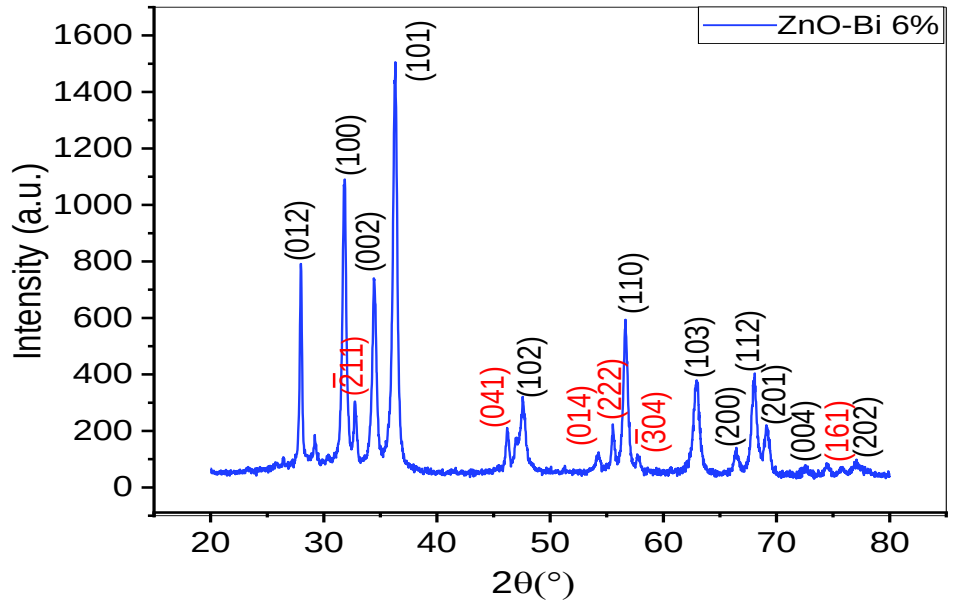

Figure III.3: XRD patterns of Bi-doped ZnO with a doping concentration of 6%.

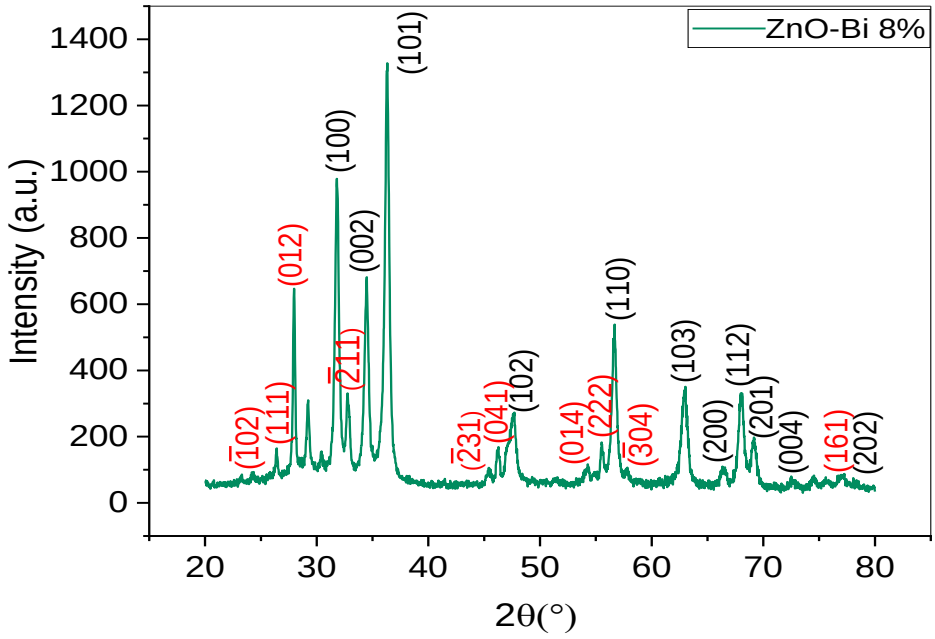

Figure III.4: XRD patterns of Bi-doped ZnO with a doping concentration of 8%.

All the observed peaks in these XRD patterns (Figure III.(1-4)) are well matched with hexagonal wurtzite structure ZnO according to the standard JCPDS card No. 36-1451 (Figure III.5).

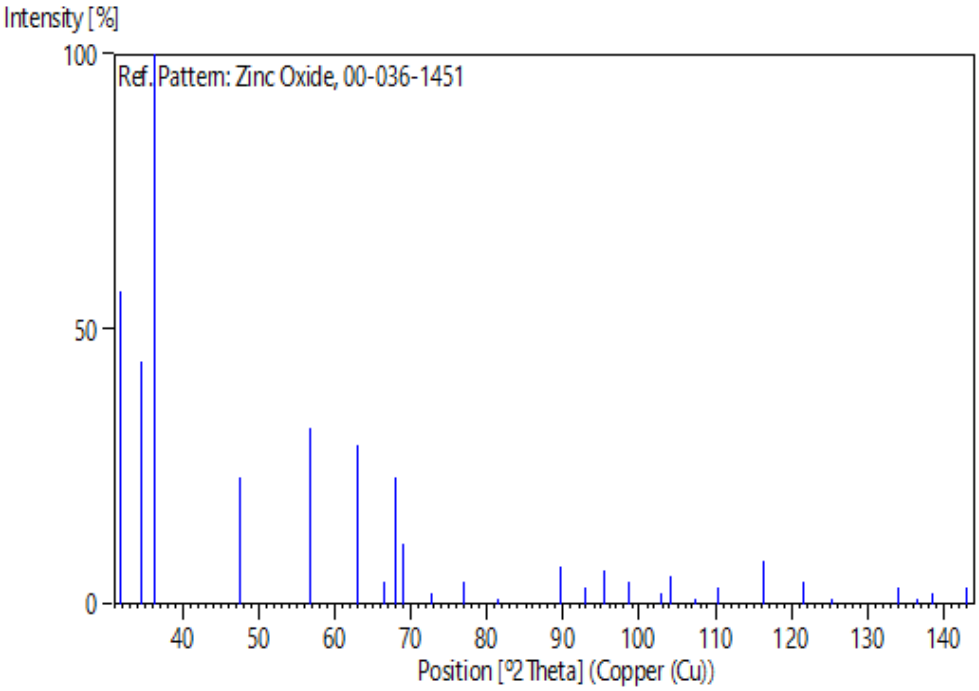

Figure III.5: Peak positions of the standard ZnO.

The XRD pattern of the samples uncovered also a solid solution for the 3% doping concentration, this result have been recorded in previous article [1-3]. No other impurity phase such as Bismuth oxide is found is due to the random substitution of Zn^{+2} by Bi^{+3} and/or the existence of Bi atoms as interstitials in the ZnO lattice [4].

In addition of ZnO main phase peaks, we have recorded peaks corresponding to the α-Bi_2O_3 monoclinic structure (JCPDS, No. 41-1449), these later have been recorded for ZnO:Bi 6% and ZnO:Bi 8% samples. These peaks indicate the appearance of the secondary phase in these samples, which may be due to the solubility limit of Bi in ZnO and only just a low quantity of this dopant could be tolerated by the ZnO structure, and consequently the excess of dopant is found as a secondary phase [5].

The appearance of this secondary phase was also reported in previous works [2, 3].The peak intensities corresponding to the α-Bi_2O_3 phase increase with the Bi content in the sample (Figure III.3 and 4) while the peak intensities corresponding to the solid solution ZnO slightly decreases as it shown in the (Figure III.6).

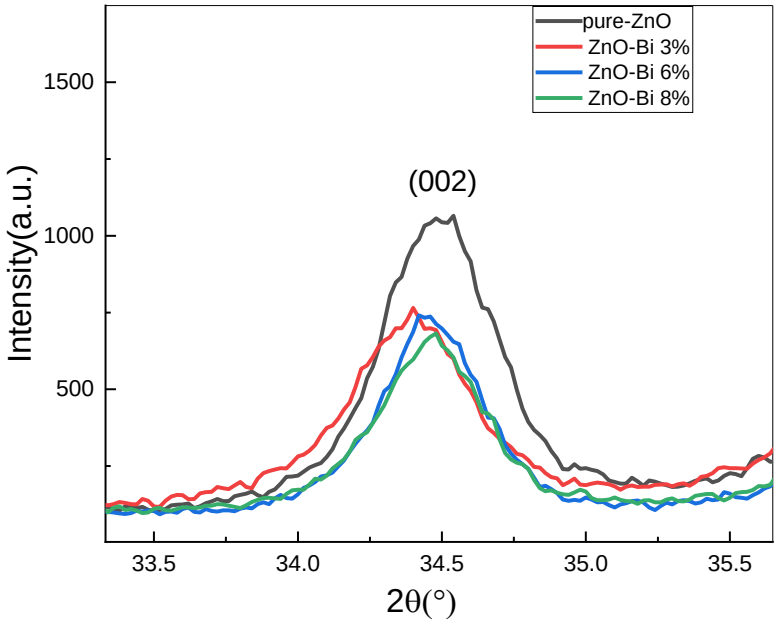

Figure III.6: Variation of the intensity of the (002) peak.

The figure (III.6) shows the intensity of the (002) peak as a function of doping concentrations. As the Bi doping level increases, the intensity of the peaks decreases gradually. We can explain this remark by the distortion in crystallinity of ZnO by substitution of the Bi dopants [1].

Also, we have noticed the appearance of new peaks with the increase of the Bi content in the samples (Figure III. 3 and 4).

At high concentrations of the Bi (6% and 8%), ZnO goes through a significant phase segregation and/or phase separation. This can be attributed to the different dimensions of two atoms, coherently with the highest ionic radius of Bi (0.103 nm) with respect to Zn (0.072 nm). In addition, Bi has a +3 charge however Zn has a +2 one, so a different content (major) of oxygen is necessary to ensure the stoichiometry of the resulting mixed oxide.

III.2.1.1. Crystallite size, lattice strain and dislocation density variation:

The crystallite size and the lattice strain of the nanoparticles was estimated using Xpert high score plus software. In this process scherrer formula (II.4) was used to calculate

Crystallite size. This formula is already stored in this software. While the dislocation density was calculated using the formula (II.7).

Table III.1: A summary table of the structural parameters of pure and Bi-doped ZnO.

Doping (%)	Crystallite size D (nm)	Lattice strain ϵ (%)	Dislocation density δ (nm^{-2})
0	34.171	0.3041	0.00085
3	28.185	0.3521	0.00125
6	57.4	0.1962	0.00030
8	32.385	0.3028	0.00095

To get the average crystallite size, we have used the peaks with high intensity, as shown below:

(100), (002), (101), (102), (110), (103) and (112). Even though Bi atoms incorporation preserves the structure of hexagonal wurtzite, which proves that the structure is still stable, the crystallite size is affected by the Bi doping. The Bi atoms incorporation in the particles network may alter the nucleation step during particle growth limiting the nucleation centers, which consequently reduces the size of the crystallites [5]. Similar behavior of decrease in the crystallite size was reported for Bi doped ZnO by Sadananda Kumar et al. [6], and in the case of Mn doped ZnO observed by Srinivasan et al. [7]. However we have recorded an increase of the crystallite size for the 6% Bi concentration (Figure III.7).

This increase can be explained, as shown in a previous paragraph, by substitution between the Bi and Zn atoms, so the difference between the ionic radius of Bi and Zn atoms, where the first one is higher than the second one, on the other hand, Bi has a +3 charge however Zn has a +2 one, so a high amount of oxygen is necessary to ensure the stoichiometry of the resulting mixed oxide.

For the 8% Bi-ZnO nanopowder, we note that the crystallite size decreases to 32,385 nm, this result can be explained by a significant phase segregation and/or phase separation, where the peaks of α-Bi_2O_3 are very clear.

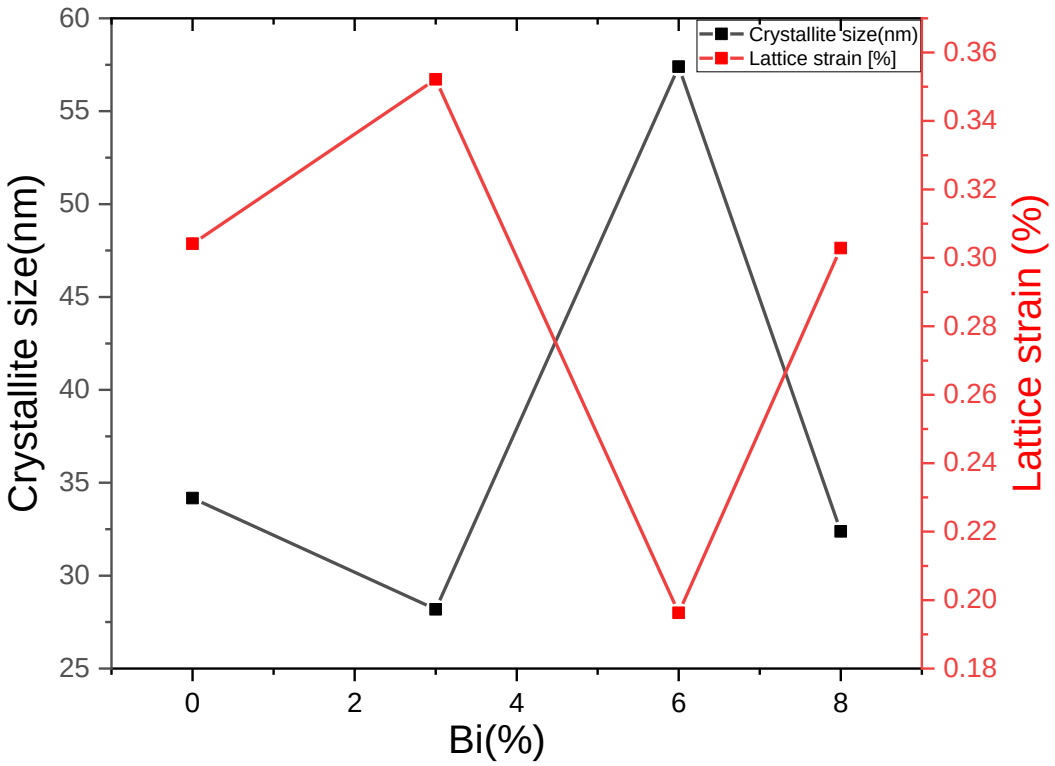

Figure III.7: Crystallite size and the strain as functions of Bi-doping.

The decrease in the crystallite size indicates an increase in the lattice defects, which in turn enhanced internal strain and dislocation density [8], as it was shown in (Figure III.7) and (Figure III.8).

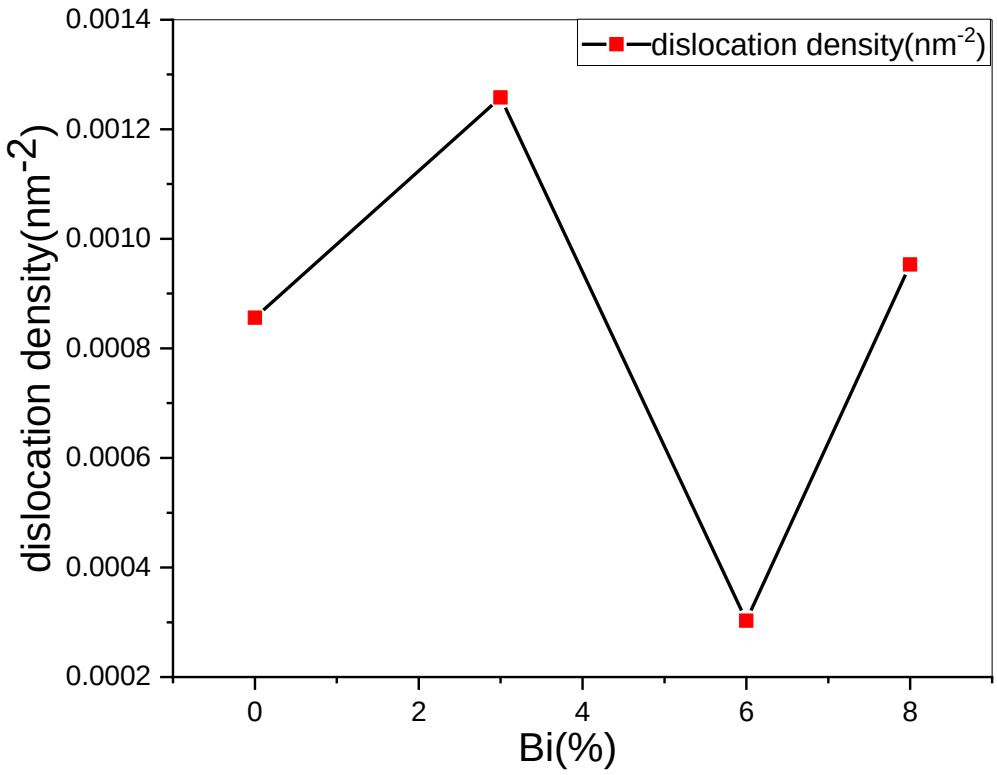

Figure III.8: The dislocation density as functions of Bi-doping.

The increase in the dislocation density can be attributed to the decrease in crystallite size. Moreover, dislocations naturally become longer as dislocation lines extend to avoid micro-structural barriers that enhanced by the decrease of crystallite size [8]. That can be the reason of the abrupt increase of dislocation density at the 3% and the 8% doping concentrations. This result can be confirmed by the crystallite size variation (figure III.7).

III.2.1.2. Lattice parameters:

The lattice constant ‘a’ and ‘c’ of the prepared samples using the (100) and (002) planes were determined using the formula (II.5).

Table III.2: Lattice parameters of pure and Bi-doped ZnO powders.

Doping (%)	$d_{(100)}$ $d_{(002)}$ (Å)	a (Å)	c (Å)	c/a
0	2.8097 2.5931	3.24441	5.18626	1.5985
3	2.8143 2.6052	3.24970	5.21044	1.6033
6	2.8086 2.6050	3.24313	5.21012	1.6065
8	2.8149 2.6020	3.25043	5.20408	1.6010

The calculated ‘a’ and ‘c’ are very close to that of the standard values up to 8 at % of Bi doping. Moreover, the ratio between the lattice constants (c/a) was estimated to be 1.60 suggesting all the prepared samples exhibit a closely packed hexagonal structure of the ZnO. Figure (III.9) presents the variation of lattice parameters, ‘a’ and ‘c’ of all the samples with Bi concentration. Both the lattice parameters, ‘a’ and ‘c’ increased with a Bi addition up to 3 at % thereby suggesting the incorporation of Bi ions into the lattice of the hexagonal wurtzite structure phase of ZnO. The cell volume expansion, which occurs when Bi^{+3} substitutes Zn^{+2} in the ZnO matrix, is expected and is based on the difference in the values of the ionic radii of the $Bi^{+}3$ and Zn^{+2} ions.

However, at higher a doping concentration (6 at %), the lattice parameter “a” has decreased. While the lattice parameter ‘c’ has slightly decreased as well. When the Bi concentration is 6 %, a larger number of Bi^{+3} ions will leave the ZnO lattice, which results in the decrease in the ZnO cell volume and lattice parameter “a”. Similar variations where reported by S. A. Ahmed when studying the structural properties of Mn-doped ZnO samples [9].

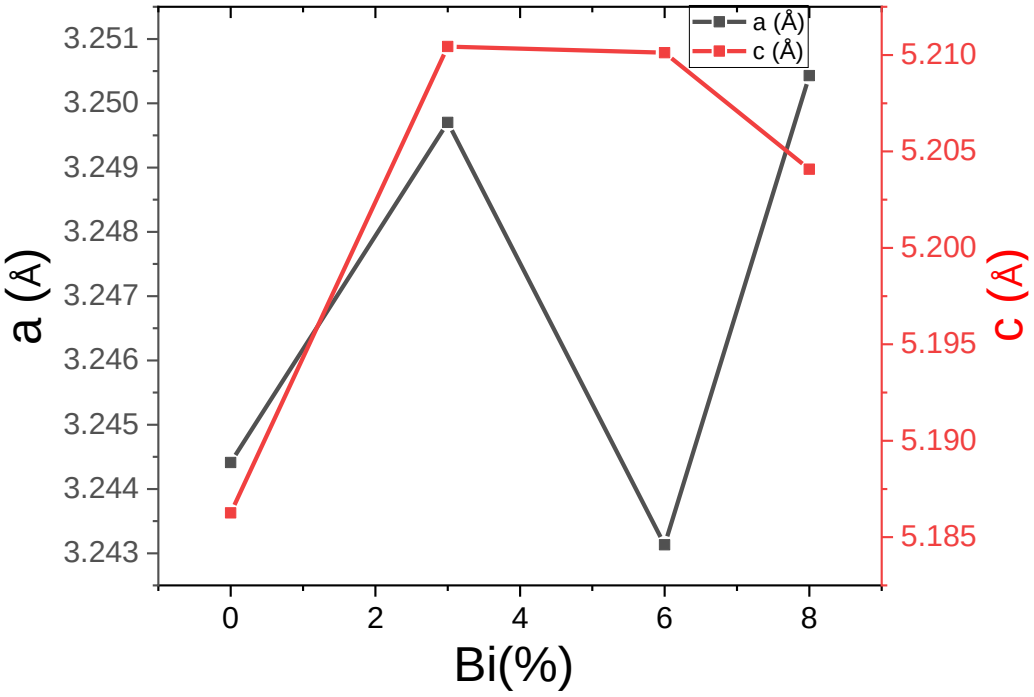

Figure III.9: Variation of lattice parameters with Bi-doping.

III.2.1.3. The texture coefficient:

To describe the growth orientation, the texture coefficient has been calculated using expression (II.8). From table (III.3) it is clear that the texture coefficient TC_{100} is the highest, which means that the direction (100) remains the preferential orientation for all doping concentrations.

Table III.3: Texture coefficient values for pure and Bi-doped ZnO.

Doping (%)	TC_{100}	TC_{002}	TC_{101}
0	1.0993	0.9678	0.9328
3	1.0713	1.0429	0.8857
6	1.1317	0.9736	0.8946
8	1.1633	0.9928	0.8439

III.2.2. Optical study:

In our study we used EVOLUTION 220 UV-VIS spectrophotometer. Transmittance spectra measured in the wavelength range from 200 to 800 nm were given in (Figure III.10).

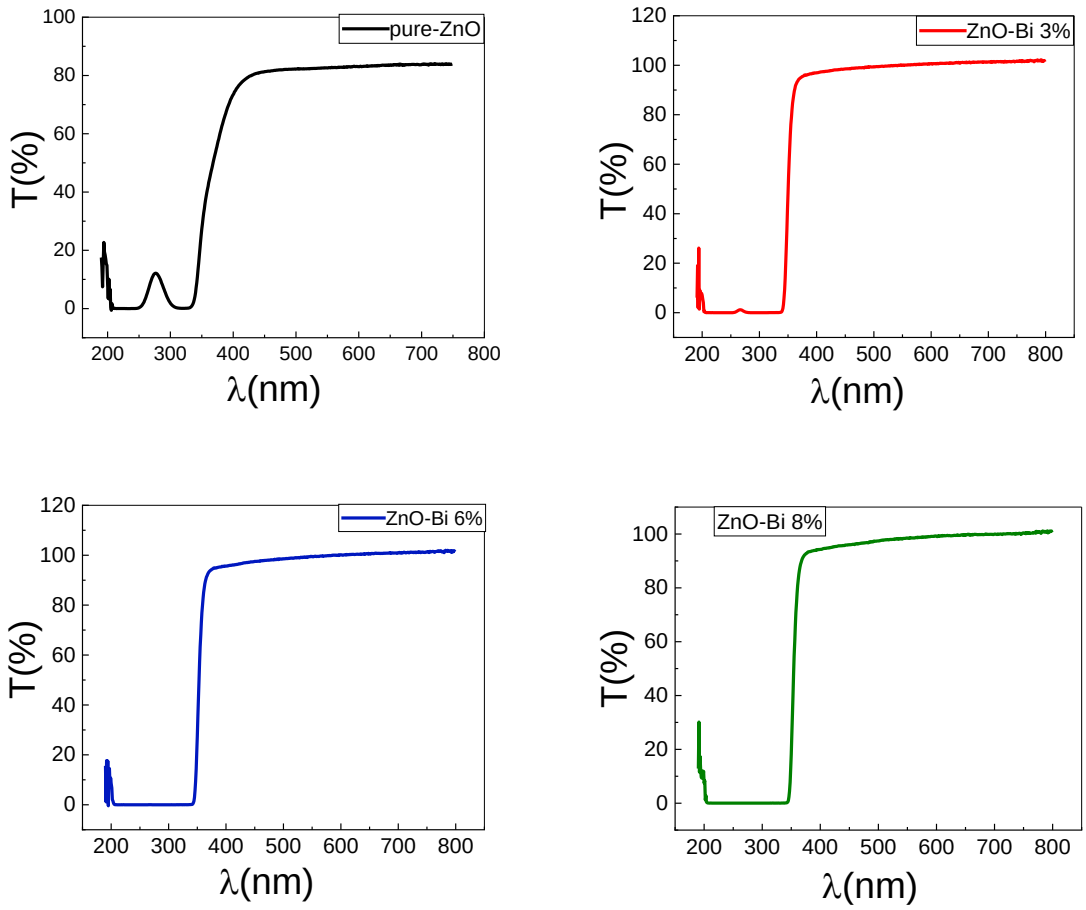

Figure III.10: The transmittance spectra of undoped and Bi doped ZnO.

One can notice that for the longer wavelengths (λ>400 nm) all the powders become transparent; it is found that all the samples show a high optical transmission, more than 80%, in the visible region. The optical absorption at the absorption edge corresponds to the transition from valence band to the conduction band (around 350 nm), while the absorption in the UV region was related to some local energy levels caused by intrinsic defects. In this region found that the transmission decreased because of the onset fundamental absorption in the region between 330–350 nm, as it is shown in the (Figure III.10), the ZnO powders

reveal strong absorption bands at 330–350 nm assigned to Zn–O bonding in wurtzite ZnO [10].

III.2.2.1. Band gap energy:

The energy gap (Eg) values depend, in general, on the crystal structure, the arrangement and distribution of atoms in crystal lattice. The optical band gap Eg of pure and Bi doped ZnO was obtained by extrapolating the linear portion of the plot $(\alpha h\nu)^2$ versus (E) (Figure III.11).

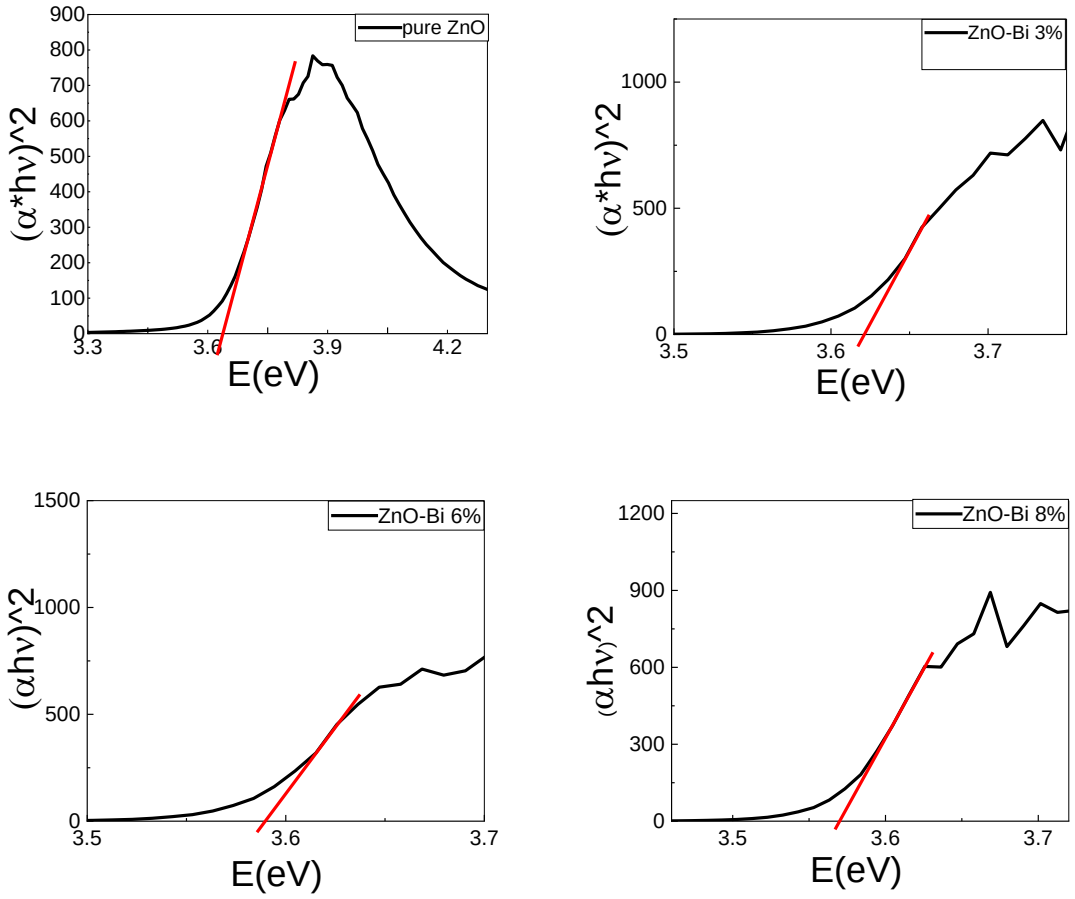

Figure III.11: Plots of $(\alpha h\nu)^2$ versus E of pure and Bi doped ZnO.

The following table (III.4) shows the optical gap of each sample.

Table III.4: Optical band gap values of undoped and Bi doped ZnO.

Doping (%)	0	3	6	8
Eg (eV)	3.633	3.620	3.587	3.569

The variation of energy band gap for pure and Bi doped ZnO powders as function of doping is presented in (Figure III.12). It can be noticed that the band gap decreased as the Bi concentration increased, which might be due to the large absorption of the sample by the effect of sp–d interaction with the localized d electrons and the Bi dopant band electrons [1].

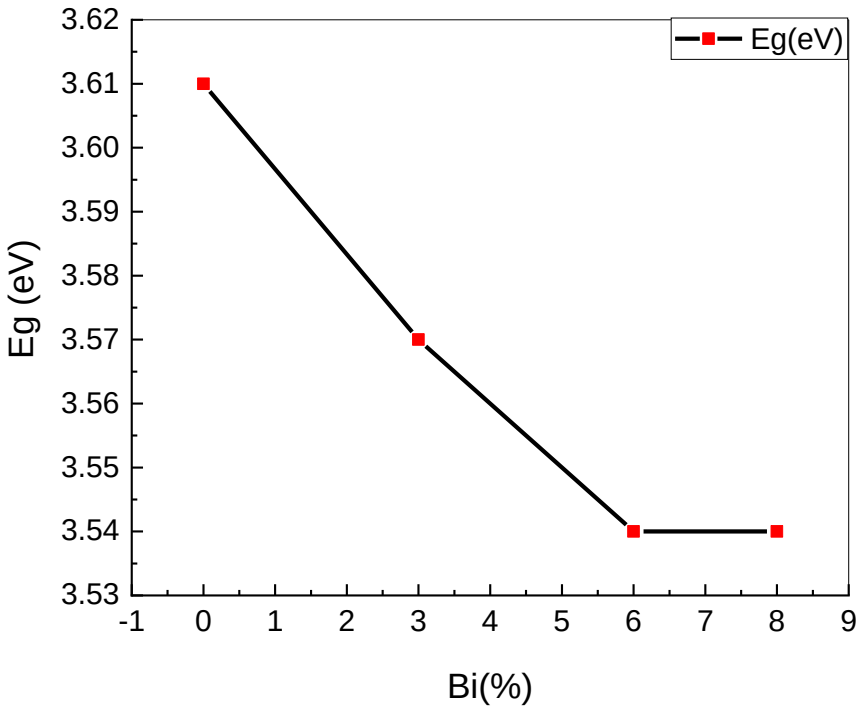

Figure III.12: Variation of the band gap with the Bi doping.

III.2.2.2. Urbach energy:

The Urbach tail is an essential parameter used to estimate the level of crystallinity and structural defect or degree of disorder present in the materials. Generally, the optical transmittance and optical band gap structure affected by the width of localized states available in the powders which are known as Urbach tail. This exponential tail appears in the

low crystalline, poor crystalline, the disordered and amorphous materials because these materials have localized states which extended in the band gap [8].

Figure shows the Ln(α) versus (hυ) for pure and Bi doped ZnO powders. The Urbach energy is estimated from the plots of Ln(α) versus E (Figure III.13) by taken the inverse of the slope of the linear part.

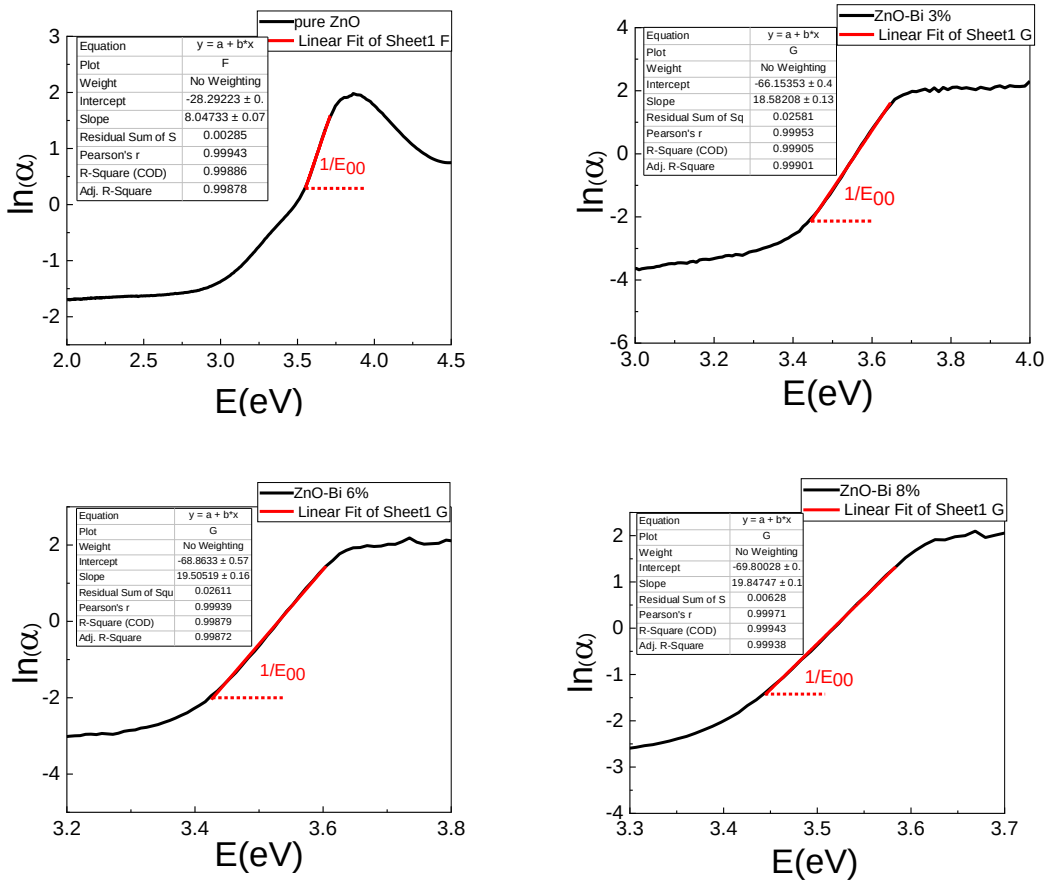

Figure III.13: Plots of ln(α) against E of pure and Bi doped ZnO.

The following table (III.5) gives the different values of the Urbach energy (Eu).

Table III.5: Urbach energy values of undoped and Bi doped ZnO.

Doping (%)	0	3	6	8
E_{00} (eV)	0.1242	0.0538	0.0512	0.0503

As shown in Figure, the Urbach energy decreases with the increases of the Bi doping. This behavior proves that the degree of structural disorder decreases with the increase of doping concentration. This may due to the improvement of crystallinity and minimization of strain and dislocation density; therefore, the defects in doped ZnO powders were reduced [8].

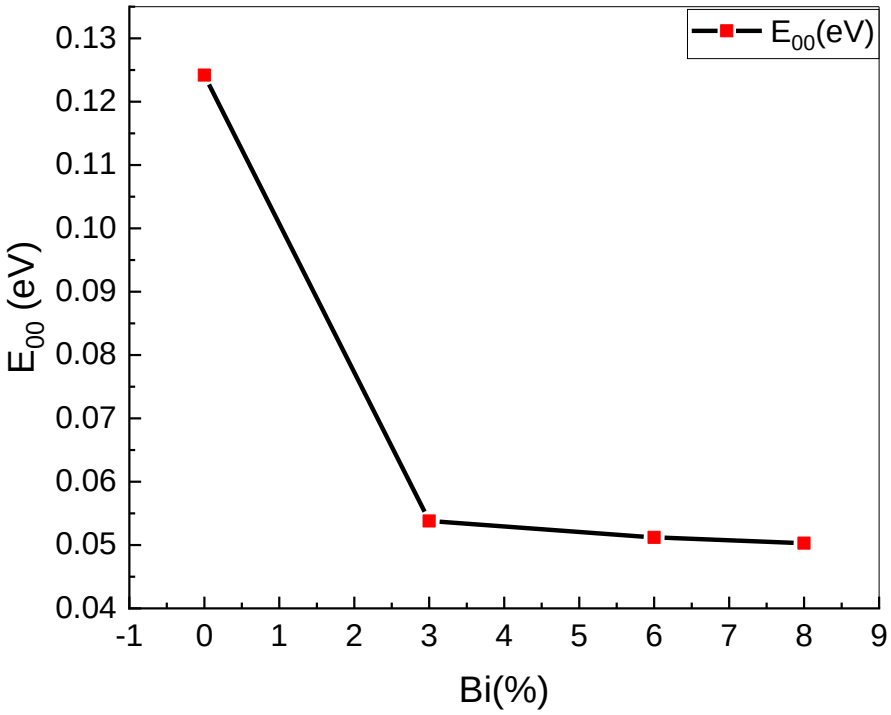

Figure III.14: Urbach energy as function of the Bi doping.

III.2.3. Chemical study:

Figure (III.15) shows the FT-IR spectrum of pure ZnO and Bi doped ZnO samples in the range 4000–400 cm^{-1}.The broad peak in the range 3434–3116 cm^{-1} corresponds to the O–H bond. The C=O bond observed at 1391 cm^{-1} is due to the presence of zinc carbonate as impurity. The carbonate probably comes from reactive carbon dioxide in the atmosphere. The

peak located at 2932 cm^{-1}, is attributed to C–H bonds that appears due to an environmental contamination. The presence of the Zn–O bond is indicated by the absorption peak at 434 cm^{-1} [5].

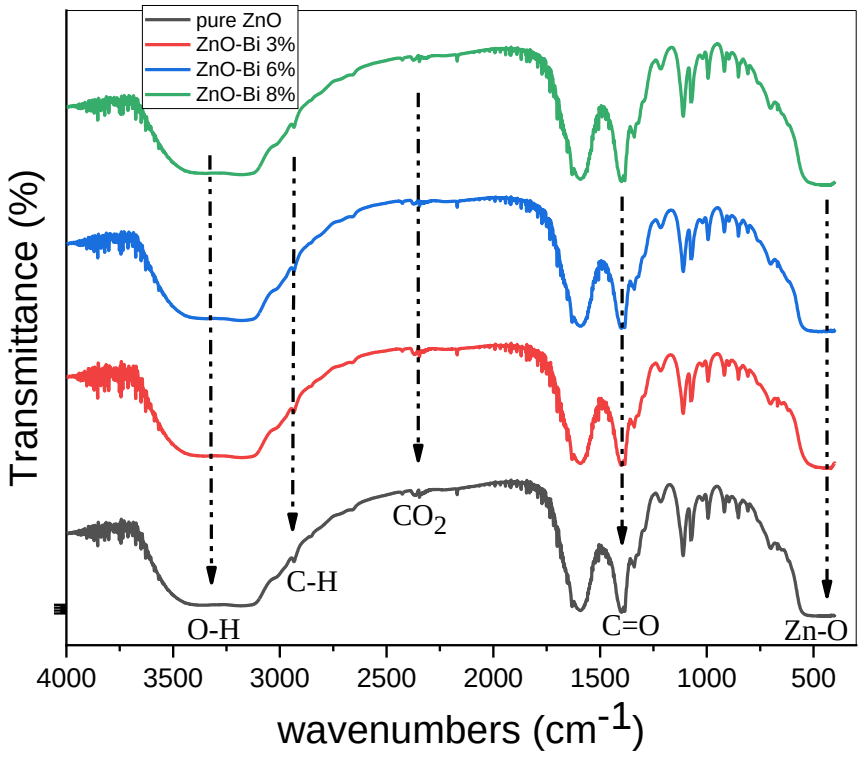

Figure III.15: FTIR spectra of undoped ZnO and Bi-doped ZnO.

References:

[1] S. Khadijah, Mohd. Al-Namshah, Shkir, S.M. Hamdy. Enhanced Hotocatalytic Performance of One-Pot Flash Combustion Synthesized ZnO Nanoparticles: An Effect of Bi Doping, Journal of Inorganic and Organometallic Polymers and Materials, vol 31, p 4338–4348, (2021).

[2] A. Boumezoued, K. Guergouri, R. Barille, D. Rechem, M. Zaabat, M. Rasheed. ZnO Nanopowders Doped with Bismuth Oxide, From Synthesis to Electrical Application, Journal of Alloys and Compounds, vol 791, p 550-558, (2019).

[3] T. Ait Ahcene, C. Monty, J. Kouam, A. Thorel, G. Petot-Ervas, A. Djemel. Preparation By Solar Physical Vapor Deposition (SPVD) and Nanostructural Study of Pure and Bi Doped ZnO Nanopowders, Journal of the European Ceramic Society, vol 27, p 3413–3424, (2007).

[4] E. Gunaid. Doctorat Thesis, Synthesis and Characterization of Zinc Oxide Nanopowder Doped with Copper by Microwave Assisted Polyol Method, University King Fahd of Petroleum & Minerals, (2012).

[5] T. Prakash, G. Neri, A. Bonavita, E. Ranjith Kumar, K. Gnanamoorthi. Structural Morphological and Optical Properties of Bi-doped ZnO Nanoparticles Synthesized by a Microwave Irradiation Method, p 4913–4921, (2015).

[6] N. Sadananda Kumar, K.V. Bangera, C. Anandan, G.K. Shivakumar, J. Alloys. Properties of ZnO: Bi Thin Films Prepared by Spray Pyrolysis Technique, vol 578, p 613–619, (2013).

[7] G. Srinivasan, J. Kumar, J. Cryst. Effect of Mn Doping on The Microstructures and Optical Properties of sol–gel Derived ZnO Thin Films, vol 310, p 1841–1846, (2008).

[8] A. Yahia. Doctorat Thesis, Optimization of Indium Oxide Thin Films Properties Prepared by sol gel Spin Coating Process for Optoelectronic Applications, University Mohamed Khider of Biskra, (2020).

[9] S. A. Ahmed. Structural, Optical, and Magnetic Properties of Mn-doped ZnO Samples, vol 7, p 604–610, (2017).

[10] F. Bouaichi. Doctorat Thesis, Deposition and analysis of Zinc Oxide thin films elaborated using spray pyrolysis for photovoltaic applications, University Mohamed Khider of Biskra, (2019).

GENERAL CONCLUSION

The main goal of this study is to investigate the effect of bismuth doping on ZnO structural and optical properties. In order to achieve that, pure and Bi-doped ZnO nanopowders with different dopant concentrations were prepared by the sol-gel method. This soft chemistry method allows obtaining powders with a good quality in a nanometric size range. The structural and optical properties of the powders have been analyzed using X-ray diffraction (XRD), UV-VIS spectroscopy and Fourier transform infrared spectroscopy (FTIR).

The XRD results confirm that the prepared samples exhibit a polycrystalline hexagonal wurtzite structure of ZnO. The crystallite size, the lattice strain, the dislocation density, and Lattice parameters are all influenced by the Bi doping.

Analysis of UV-VIS spectra revealed that the band gap decreased from 3.63 to 3.56 eV, as the Bi concentration increased. The Urbach energy Also decreased gradually revealing that the higher Bi doping rate may have caused an improvement in crystallinity.

FTIR spectra confirmed the presence of the Zn–O bond for all samples. While The C=O and C–H bonds appear due to the environmental conditions.

In summary, the simple synthesis method proposed represents an interesting approach to producing Bi-doped ZnO nanopowders, with promising potential for optical applications.
It is also worth noting that we can take into account some different perspectives to complete this work such as:

* Some additional characterizations that could still be made (SEM, TEM, and I(V) electrical measurements).
* Doping and co-doping ZnO powders with other elements such as Cu…etc.
* Integrating the doped powders in one of the multiple uses such as varistors or photocatalytic application.

ABSTRACT

In this work, undoped and Bi-doped ZnO nanopowders with different dopant concentrations (3%, 6% and, 8%) have been successfully synthesized with a soft chemistry method: the sol-gel route. This method produces samples with high purity, homogeneity, and a structure of easy control. The powders have been characterized using the following techniques: X-ray diffraction (XRD), UV–visible spectroscopy (UV–vis), and Fourier transform infrared (FTIR) spectroscopy.

The XRD results confirm that all the samples exhibit a polycrystalline hexagonal wurtzite structure of the ZnO. The crystallite size was found to vary between 28.1 and 57.4 nm. The results of UV analysis showed a decrease in the values of the band gap energy (Eg) and the Urbach energy with the increase of the Bi doping concentration. In addition, Fourier transforms infrared (FTIR) spectroscopy showed the presence of a zinc oxide-specific bond in the samples. The simple synthesis method proposed represents an interesting approach to produce Bi-doped ZnO nanopowders, with promising potential for different applications.
Keywords: zinc oxide, Bismuth, nanopowder, sol-gel, XRD, UV–vis, FTIR.

ملخص

في هذا العمل، تم تصنيع المساحيق النانوية من أكسيد الزنك غير المطعمة والمطعمة بتركيزات مختلفة من البيسميث (3٪ و6٪ و8٪) بنجاح باستخدام طريقة كيميائية: تقنية محلول-هلام. تنتج هذه التقنية عينات عالية النقاء والتجانس وبنية يسهل التحكم فيها. تم تشخيص المساحيق باستخدام التقنيات التالية: انعراج الأشعة السينية (XRD) والتحليل الطيفي للأشعة فوق البنفسجية المرئية (UV–vis) والتحليل الطيفي للأشعة تحت الحمراء (FTIR).

تؤكد نتائج انعراج الأشعة السينية أن جميع العينات تظهر بنية سداسية متراصة متعددة البلورات لأكسيد الزنك. وجد أن حجم البلورات يتراوح بين 28.1 و57.4 نانومتر. أظهرت نتائج تحليل الأشعة فوق البنفسجية انخفاضًا في قيم طاقة النطاق الممنوع (Eg) وطاقة أورباخ مع زيادة التطعيم. بالإضافة إلى ذلك، أظهر التحليل الطيفي للأشعة تحت الحمراء وجود رابطة خاصة بأكسيد الزنك في كل العينات. طريقة التحضير البسيطة المقترحة تمثل نهجًا مثيرًا للاهتمام لإنتاج مساحيق نانوية لأكسيد الزنك المطعمة بالبيسميث، مع إمكانية استخدامها في تطبيقات مختلفة.

الكلمات المفتاحية: أكسيد الزنك، البيسميث، المساحيق النانوية، محلول-هلام، انعراج الاشعة سينية، مطيافية فوق البنفسجي- المجال المرئي، مطيافية ما فوق الحمراء.